Lactobacillus plantarum R-fermented Phellodendron amurense extract protects against PRV infection in vitro and in vivo by modulating oxidative stress and inflammatory responses

Mengyao Zhao
College of Veterinary Medicine, Henan Agricultural University
feifan Wu
College of Veterinary Medicine, Henan Agricultural University
zenghao Xu
College of Veterinary Medicine, Henan Agricultural University
xing Han
College of Veterinary Medicine, Henan Agricultural University
sai Mao
College of Veterinary Medicine, Henan Agricultural University
hongying Zhang
College of Veterinary Medicine, Henan Agricultural University
yina Zhang
College of Veterinary Medicine, Henan Agricultural University
mingfan Yang
yangmingfan123@163.com

College of Veterinary Medicine, Henan Agricultural University

Research Article

Keywords: probiotic fermentation, postbiotics, pseudorabies virus (PRV), oxidative stress, inflammation, feed additive, swine health

Posted Date: May 8th, 2026

DOI: https://doi.org/10.21203/rs.3.rs-9563893/v1

Additional Declarations: No competing interests reported.

Version of Record: A version of this preprint was published at Probiotics and Antimicrobial Proteins on August 5th, 2026. See the published version at https://doi.org/10.1007/s12602-026-11147-y.

Abstract

Pseudorabies virus (PRV) infection poses a significant health challenge to swine production, inducing oxidative stress, inflammatory responses, and reduced growth performance. Probiotic fermentation of medicinal plants is a promising strategy for generating novel probiotic-derived products for improving animal health. In this study, Phellodendron amurense (PA), a plant with both medicinal and dietary applications, was fermented with Lactobacillus plantarum R (LpR). We investigated the potential of fermented extract (FPAE) as a probiotic-derived feed additive for swine and its underlying mechanisms. Nontargeted UPLC–MS/MS metabolomics revealed that fermentation significantly reshaped the metabolic profile of PAs, with marked enrichment of phenolic acids, flavonoids, and alkaloids. Specifically, the berberine content increased 2.5fold, and the levels of antioxidant components such as ferulic acid and kaempferol were significantly increased. In vitro, FPAE inhibited PRV replication in PK15 cells in a concentrationdependent manner (84.15% inhibition at 5 mg/mL). It also alleviated virusinduced oxidative stress, as evidenced by restored glutathione peroxidase (GSHPx) and superoxide dismutase (SOD) activities and reduced malondialdehyde (MDA) levels. The supernatant of LpR showed no antiviral activity, confirming that the enhanced efficacy resulted from biotransformation of the plant matrix. In vivo, daily oral administration of FPAE (125 mg/mL, 200 μL/mouse, equivalent to 892 mg/kg) significantly improved the survival rate (80% vs. 53.33% in the model group); increased the average daily weight gain and feed conversion ratio; reduced the viral loads in the brain, lung, spleen and kidney; and alleviated pathological damage to the brain and clinical symptoms. Furthermore, FPAE suppressed systemic inflammatory responses (decreased serum IL6, $P < 0.05$) and enhanced antioxidant defense (increased GSHPx activity, $P < 0.05$). Through a multidimensional “constituent–cell–animal” approach, this study demonstrated that probiotic fermentation restructures the chemical composition of Phellodendron amurense and synergistically regulates host oxidative stress and inflammatory responses to confer protection against viral infection. These findings provide a theoretical basis for developing LpRfermented Phellodendron amurense as a functional feed additive to control PRV infection in swine.

Introduction

Pseudorabies virus (PRV) is a significant member of the α-herpesvirus subfamily within the Herpesviridae family, causing pseudorabiasis (PR) in pigs. This disease poses a persistent and severe economic threat to the global swine industry. PRV has a broad host range, causing nearly 100% mortality in piglets while establishing lifelong latent infections in surviving herds, thereby becoming a potential source for sustained viral transmission[1, 2]. More critically, PRV can be transmitted between species, with documented infections in various mammals, including cattle, dogs, and cats[3]. Recent epidemiological evidence suggests a potential risk of human infection, raising significant public health concerns[4, 5].

Although the widespread use of live attenuated vaccines (such as the Bartha-K61 strain) has resulted in partially controlled outbreaks, antigenic variants of PRV have emerged successively in China and Southeast Asia since 2011, significantly reducing the protective efficacy of existing vaccines[6, 7].

Molecular epidemiological studies have revealed that these variants harbor multiple mutations in immunologically relevant glycoprotein regions, such as gC and gE, potentially altering viral antigenicity and enabling partial escape from vaccine-induced immune responses[8]. This situation underscores the urgency of developing novel, complementary antiviral strategies—particularly multitarget interventions that do not rely on specific immune recognition and are less prone to inducing viral resistance.

Natural products, especially bioactive compounds derived from medicinal plants, have become crucial sources of antiviral lead compounds because of their multicomponent, multitarget synergistic effects, low toxicity, and resistance to developing drug resistance[9, 10]. Extensive research has confirmed the antiviral activity of plant-derived compounds. For example, the photosensitive natural product phopeophorbide a (Pba) directly targets the viral particles of enveloped viruses, such as coronaviruses, under light exposure[11]. It inhibits virus—cell membrane fusion by stiffening the viral envelope, thereby blocking viral entry into cells. Berbamine (BBM) significantly inhibits influenza A virus (IAV) infection by suppressing viral adsorption and entry during early infection stages while modulating host inflammatory responses to mitigate virus-induced immunopathological damage[12]. These examples not only highlight the potential of plant-derived compounds as antiviral agents but also suggest that their mechanisms often involve the systematic regulation of virus—host interaction networks.

Among the numerous bioactive plant resources, *Phellodendron amurense* (Huang Bai), a traditional medicinal and edible plant, has a long history of culinary and medicinal use in Asia[13]. *Phellodendron amurense* is rich in diverse bioactive components, including alkaloids (e.g., berberine, palmatine, and eupatorine), flavonoids (e.g., phellodendrin, kaempferol, and quercetin), and phenolic acids (e.g., ferulic acid and chlorogenic acid). Modern pharmacological studies indicate that these components exhibit multiple biological activities, including anti-inflammatory, antioxidant, antibacterial, hepatoprotective, and neuroprotective effects[14, 15]. Notably, *Phellodendron amurense* extract has been demonstrated to inhibit various viruses, including influenza, hepatitis, and herpes viruses. As a characteristic alkaloid of Phellodendron, the antiviral mechanisms of berberine have been partially elucidated and involve multiple mechanisms, including the inhibition of viral replication, the modulation of host immune responses, and the alleviation of oxidative stress induced by viral infection[16-18].

However, the application of traditional *Phellodendron amurense* water extracts faces several bottlenecks. First, key active components, such as berberine, exhibit poor water solubility and low intestinal absorption, with oral bioavailability below 5%[19]. Second, the complex constituents in the extract may undergo degradation or transformation in the gastrointestinal environment, resulting in effective concentrations reaching target organs that are significantly lower than those observed in in vitro experiments[20]. Furthermore, conventional water extraction processes struggle to release functional components bound to cell walls fully, thereby limiting their potential activity[21]. These inherent limitations severely constrain the in vivo efficacy of Phellodendron amurense water extracts and hinder their large-scale application as functional foods or feed additives.

In recent years, probiotic fermentation has garnered significant attention in food science and functional food research as a green bioconversion technology[22, 23]. This technology utilizes enzyme systems (e.g., β-glucosidase, esterase, cellulase) produced by food-grade microorganisms such as *Lactobacillus* and Bacillus during their growth and metabolism in plant substrates. These enzymes catalyze the biotransformation of macromolecular compounds in plant matrices into smaller-molecular-weight metabolites with increased bioavailability[24, 25]. This process may increase the health benefits of plant-based foods through multiple mechanisms: (1) converting bound glycosides into free aglycones, improving intestinal absorption; (2) hydrolyzing cell wall polysaccharides to release intracellular functional components; (3) generating new bioactive substances via microbial metabolism; and (4) reducing or eliminating antinutritional factors or toxic components in raw materials. Previous studies have demonstrated that various plant-based foods (e.g., soybeans, kudzu roots, and goji berries) exhibit significant increases in antioxidant and anti-inflammatory activities after *Lactobacillus* fermentation[26-28], which is closely linked to the restructuring of their compositional profiles during fermentation[29-31]. However, research systematically investigating how specific probiotic fermentations modify the chemical profiles of plant matrices and how these changes are mechanistically related to antiviral functions remains limited.

Preliminary screening in this study revealed that among various fermented herbal extracts, the Phellodendron amurense water extract fermented by LpR presented the most pronounced in vitro anti-PRV activity. On the basis of these findings, we propose that LpR fermentation enhances defense against PRV infection by restructuring the chemical composition of *Phellodendron amurense*, enriching antioxidant and anti-inflammatory active components, and synergistically regulating host oxidative stress and inflammatory responses. Metabolomic technology was employed to analyze compositional changes before and after fermentation. Combined with validation through cellular and animal models, this study aims to provide a theoretical basis for developing probiotic-fermented plant-based feed additives.

Materials and methods

1.1 Medicinal materials, strains, and reagents

Phellodendron amurense (PA) was purchased from Zhengzhou Zhongjing Pharmacy (China) and used as the plant-based fermentation substrate. The probiotic strain LpR was isolated, identified, and stored in our laboratory from traditional kimchi. The Pseudorabies virus (PRV) NY strain (GenBank accession number: KF130883) was kindly provided by a collaborating laboratory. Porcine kidney cells (PK-15) were maintained in our laboratory. Cell culture was performed with DMEM purchased from Beijing Solabio Technology Co., Ltd. (China) and fetal bovine serum (FBS) purchased from Hangzhou Sijiqing Biological Engineering Materials Co., Ltd. (China). Cell viability was assessed via a Cell Counting Kit-8 (CCK-8, A311, Vazyme, China). Viral genomic DNA was extracted via the E.Z.N.A.® Blood DNA Kit (D3392-02, Omega Biotek, USA). Real-time quantitative PCR (qPCR) was performed with a SYBR® Green Premix Pro Taq HS qPCR Kit (AG11701, Accurate Biology, China). Antioxidant marker assay kits, including

glutathione peroxidase (GSH-Px, Cat No. A005-1-2), superoxide dismutase (SOD, Cat No. A001-3), and malondialdehyde (MDA, Cat No. A003-1), were purchased from Nanjing Jiancheng Bioengineering Institute (China). The mouse inflammatory cytokines IL-6 and IL-1β were detected via enzyme-linked immunosorbent assay (ELISA) kits (Mouse IL-6 Uncoated ELISA Kit, Cat No. 88-7064-88; Mouse IL-1β Uncoated ELISA Kit, Cat No. 88-7013-88; Thermo Fisher Scientific, USA). Chromatography-grade reagents for metabolomics analysis, including methanol (Cat No. 1.06007.4000, Merck, Germany), acetonitrile (Cat No. A433531-100 ml, Aladdin, China), formic acid (Cat No. F112036-500 g, Aladdin, China), and ammonium formate (Cat No. A100185-250 g, Aladdin, China), were purchased from Merck (Germany) and Aladdin (China).

1.2 Sample Preparation

This study prepared and analyzed the following three samples: (1) Phellodendron amurense extract (PAE), (2) fermented PAE (FPAE), and (3) LpR supernatant (LpS). The specific preparation procedures are shown in Figure 1. The prepared PAE, FPAE, and LpS were filtered with a 0.22 μm membrane in a laminar flow hood, aliquoted, and stored at -80°C for subsequent experiments. The PAE was prepared as a concentrated solution containing 1 g of crude drug per milliliter for subsequent fermentation and cell experiments. For the animal experiments, PAE or FPAE was diluted with distilled water to the desired concentration and administered via gastric gavage.

1.3 Assessment of LpR growth in the Phellodendron amurense matrix

The activated LpR seed culture was inoculated at 4% (v/v) into fresh sterile PAE (1 g crude drug/mL) and fermented statically at 37°C. The sterile samples were collected at 0 h and 48 h postfermentation. The live bacterial concentration was determined via the plate count method. The samples were tenfold diluted, and an appropriate dilution was spread onto de Man, Rogosa and Sharpe (MRS) agar plates. The plates were incubated anaerobically at 37°C for 48 h. Colony-forming units (CFUs) were counted, and the live bacterial concentration (CFU/mL) was calculated.

1.4 Metabolomic analysis

Nontargeted metabolomics analysis was performed on three sample groups—PAE, FPAE, and LpS—with ultraperformance liquid chromatography-tandem mass spectrometry (UPLC-MS/MS). Fifty microliters of each sample was mixed with 150 μL of prechilled extraction buffer containing internal standards (methanol:acetonitrile = 1:1, v/v). The mixture was vortexed for 3 minutes and centrifuged at 12,000 ×g for 10 minutes at 4°C. The supernatant was allowed to stand at -20°C for 30 minutes to precipitate the proteins. After centrifugation, the supernatant was collected for analysis. Chromatographic separation was performed on a Thermo Scientific™ Vanquish™ system equipped with an ACQUITY UPLC HSS T3 column (1.8 μm, 2.1 mm × 100 mm). Mobile phase A was 0.1% formic acid in water, and mobile phase B was 0.1% formic acid in acetonitrile. The column temperature was maintained at 40°C, the flow rate was 0.4 mL/min, and the injection volume was 4 μL. The following gradient elution program was used: 0–2.0 min, 5% B; 2.0–5.0 min, 5–60% B; 5.0–6.0 min, 60–99% B; 6.0–7.5 min, 99% B; 7.5–7.6 min, 99–5% B;

and 7.6–10.0 min, 5% B. Mass spectrometry analysis was performed on a Thermo Scientific™ Q Exactive™ HF-X mass spectrometer using an electrospray ionization source, with data acquired in both positive and negative ion modes. The spray voltages were set at +3.5 kV and -3.2 kV, with an ion transfer tube temperature of 320°C. The raw MS data were converted to the .mzXML format via ProteoWizard, followed by peak extraction, retention time correction, and peak alignment via the XCMS software package. Metabolites were identified via comparisons against in-house databases and public repositories, including HMDB and MassBank. Multivariate statistical analysis was performed via SIMCA-P software. Principal component analysis (PCA) was first used to assess overall data quality and trends in intergroup separation. Orthogonal partial least squares discriminant analysis (OPLS-DA) models were then constructed to maximize intergroup differences, and model quality was validated via R^2 and Q^2 values. The selection criteria were set as follows: variable importance projection (VIP) > 1.0 and Student's t test P value < 0.05. Kyoto Encyclopedia of Genes and Genomes (KEGG) pathway enrichment analysis was performed on the selected differentially abundant metabolites to elucidate potential biological metabolic pathways affected by the fermentation process. Quality control samples were included in all analyses to monitor system stability.

1.5 Cell culture and virus propagation

PK-15 cells were routinely cultured in DMEM supplemented with 10% heat-inactivated fetal bovine serum (FBS) and 1% penicillin–streptomycin dual antibiotics at 37°C in a humidified incubator with 5% CO_2. The cells were passaged every 2–3 days and digested with 0.25% trypsin-EDTA solution when the confluence reached 80–90%.

The PRV-NY strain was propagated in PK-15 cells. The cells were seeded in culture flasks and allowed to grow to approximately 80% confluence. The medium was then removed, and the cells were washed twice with PBS. An appropriately diluted virus inoculum (infection titer ≈ 0.1 MOI) was added and allowed to adsorb for 1 hour at 37°C, after which the flasks were gently shaken every 15 minutes. After adsorption, maintenance medium containing 2% FBS was added, and the culture was continued. The cytopathic effect (CPE) was observed daily. When approximately 80% of the cells exhibited typical lesions (cell rounding and detachment), the culture was frozen at -80°C. The cells were subsequently subjected to three freeze–thaw cycles to lyse the cells and release the virus. The cell debris was removed by centrifugation at 4°C and 3000 ×g for 10 minutes. The viral supernatant was aliquoted and stored at -80°C for future use.

1.6 Cytotoxicity Assay

To determine the safe working concentration ranges of PAE, FPAE, and the positive control, vitamin C (VC), for PK-15 cells, cytotoxicity was assessed with the CCK-8 assay. Log-phase PK-15 cells were seeded at a density of 1×10^4 cells per well in a 96-well plate and cultured at 37°C with 5% CO_2 for 24 hours until confluence. The original culture medium was removed, and solutions of PAE, FPAE (concentration gradient: 10, 5, 2.5, 1.25, 0.625, 0.3125 mg/mL) or vitamin C (concentration gradient: 50, 25, 5, 2.5, 1.25, 0.625 μg/mL) were added. Each concentration was tested in 5 replicate wells, with a

blank control group containing only medium and a drug-free cell control group. Cultures were maintained for an additional 24 hours post-treatment. Subsequently, 10 μL of CCK-8 solution was added to each well and incubated in a dark incubator for 2 hours. The absorbance values at 450 nm were measured via a multifunctional microplate reader.

Cell viability was calculated via the following formula: cell viability (%) = [($OD_{(}$drug group$_{)}$ – $OD_{(}$blank group$_{)}$)/($OD_{(}$cell control group$_{)}$ – $OD_{(}$blank group$_{)}$)] × 100%. The maximum drug concentration yielding >95% cell survival was defined as the noncytotoxic concentration and used as the upper safe limit for subsequent in vitro antiviral assays. All experiments were independently replicated three times.

1.7 Determination of tissue culture infectious dose 50 ($TCID_{50}$)

PK-15 cells were seeded at a density of 1 × 10^4 cells per well in a 96-well plate and cultured until a confluent monolayer formed. The stock virus solution was serially diluted 10-fold (10^{-1} to 10^{-8}) in DMEM maintenance medium containing 2% FBS. The medium in each well was discarded, and the wells were washed once with sterile PBS. Eight replicate wells per dilution of 100 μL per well were inoculated, including a cell control well. The mixture was incubated at 37°C in a 5% CO_2 incubator. The CPE was observed daily for 5 consecutive days. Wells exhibiting typical CPEs were considered positive for infection. The viral $TCID_{50}$ was calculated via the Reed–Muench method.

1.8 In vitro antiviral activity assay

On the basis of the safety concentration determination results, the number of viral genome copies in cells after drug treatment was quantified via qPCR. PK-15 cells were seeded in 24-well plates and pretreated for 4 hours with serial concentrations (5, 2.5, 1.25, or 0.625 mg/mL) of PAE, FPAE, LpS, or positive control VC upon reaching 70–80% confluence. After the drug mixture was discarded and the mixture was washed with PBS, each well was inoculated with 100 $TCID_{50}$ of PRV virus suspension (diluted in DMEM containing 2% FBS) and incubated for 2 hours at 37°C to allow for adsorption. Following adsorption, the virus mixture was discarded and replaced with maintenance medium containing the corresponding drug concentration for continued culture. The cells and supernatants were collected at 24, 48, and 72 hours post-infection and stored at -80°C. Viral, cell, and drug solvent controls were established concurrently. Total cellular DNA was extracted via the Omega Viral DNA Kit. Specific primers targeting the conserved region of the PRV gE gene were designed and synthesized by Wuhan Beiyinlai Biotechnology Co., Ltd. The primer sequences were as follows: forward primer (PRV-gE-F): 5'-TCGCCGAGAACTTTACC-3', reverse primer (PRV-gE-R): 5'-TAGATGCAGGGCTCTGACA-3'. The expected amplification fragment length was 92 bp. An absolute quantitative standard curve was established using gradient-diluted recombinant plasmid standards. qPCR was performed on a Bio-Rad CFX96 system with a 20 μL reaction volume: 10 μL SYBR Green Premix, 0.4 μL each forward and reverse primer, 2 μL DNA template, and 7.2 μL ddH_2O. The reaction conditions were as follows: 95°C predenaturation for 3 min; denaturation at 95°C for 10 s; annealing at 60°C for 30 s; and 40 cycles. The Ct values were converted to viral genome copies per μg of total cellular DNA on the basis of the standard curve, and the viral

suppression rate was calculated as follows: suppression rate (%) = [1 – (drug-treated group copies/viral control group copies)] × 100%. All experiments were independently replicated three times.

1.9 Detection of Cellular Oxidative Stress Markers

Cell samples were collected at 24, 48, and 72 hours post-infection. After being washed with prechilled PBS, the cells were lysed with lysis buffer on ice for 30 minutes. The supernatants were collected via centrifugation at 12,000 ×g for 10 minutes at 4°C to obtain total cellular protein extracts. The protein concentration was measured via the BCA method for data normalization.

Commercially available kits were used to determine the following indicators according to the manufacturer's instructions: (1) glutathione peroxidase (GSH-Px) activity, measured via the DTNB colorimetric assay, expressed as U/mg prot; (2) superoxide dismutase (SOD) activity, measured via the WST-1 assay, expressed as U/mg prot; and (3) malondialdehyde (MDA) content, measured via the thiobarbituric acid (TBA) method, with results expressed as nmol/mg prot. The absorbance was read via an enzyme-linked immunosorbent assay (ELISA) reader. All experiments were independently replicated three times.

1.10 Experimental animals and ethics

The SPF-grade female Kunming mice (6–8 weeks old, weighing 28 ± 2 g) used in the in vivo experiments were purchased from the Henan Provincial Laboratory Animal Center. All the animal experimental protocols were reviewed and approved by the Animal Welfare and Ethics Committee of Henan Agricultural University (Approval No. HNND2024030728). The mice were acclimated for one week under standard conditions (temperature, 22 ± 2°C; humidity, 50 ± 10%; 12-hour light—dark cycle) with free access to food and water.

1.11 PRV challenge dose and drug safety screening

To determine the median lethal dose (LD_{50}) of PRV, 48 mice were randomly divided into 6 groups (n=8). Each group received an intramuscular injection of 10-fold serially diluted PRV stock (10^{-1}, 10^{-2}, 10^{-3}, 10^{-4}, 10^{-5}, and 10^{-6} dilutions) or an equal volume of PBS. The survival rate of the mice was continuously monitored for 7 consecutive days. To determine the maximum safe dose of PAE or FPAE, 80 mice were randomly divided into 10 groups (n=8). Each group received once-daily oral gavage of PAE or FPAE at crude drug concentrations of 125, 250, 500, or 1000 mg/mL, with a fixed volume of 200 μL per mouse. On the basis of an average body weight of 28 g, these corresponded to daily doses of 892, 1784, 3568, and 7136 mg crude drug/kg body weight, respectively (e.g., 125 mg/mL × 0.2 mL/0.028 kg ≈ 892 mg/kg). The drug was administered for 7 consecutive days, during which the mice were monitored for signs of toxicity. No mortality or overt toxicity was observed at any dose, confirming the safety of the tested doses for subsequent in vivo experiments.

On the basis of the body surface area conversion formula (FDA guidelines), the daily dose of 892 mg/kg in mice (calculated as a crude drug) is equivalent to approximately 4.34 g of raw *Phellodendron*

amurense crude drug ingested daily by a 60 kg adult. This dose falls within the range of traditional dietary applications (*Phellodendron amurense* is a food-medicine dual-use plant, with daily usage typically 3–10 g), suggesting that the doses used in this study have potential for clinical translation.

1.12 Animal experimental design

On the basis of the established challenge dose and safe drug dose, 90 female Kunming mice were randomly divided into 6 groups (n=15):

Blank control group: Normal feeding without intervention

PRV model group: PRV challenge without drug intervention

PAE group: PRV challenge + daily oral administration of PAE (125 mg/mL, 200 μL/mouse), equivalent to a daily dose of 892 mg/kg body weight;

FPAE group: PRV challenge + daily oral administration of FPAE (125 mg/mL, 200 μL/mouse), equivalent to a daily dose of 892 mg/kg body weight;

LpS group: PRV challenge + daily oral administration of LpR bacterial suspension (1.1×10^7 CFU/mL, 200 μL/mouse);

VC group: PRV challenge + daily oral administration of vitamin C solution (10 mg/mL, 200 μL/mouse). The dosage of 10 mg/mL was set on the basis of prior studies[32], equivalent to a daily dose of 71 mg/kg. This dosage was confirmed in preliminary experiments to be nontoxic to mice and to possess antioxidant activity.

All treatment groups received daily oral administration starting on day 1 of the experiment, which continued until day 20. On Day 9, the mice in all the groups except those in the blank control group received intramuscular injections of a 100-fold diluted PRV-NY virus solution (100 μL/mouse) into the right hind limb. The blank control group received an equal volume of DMEM. Postchallenge, daily body weight and feed intake were recorded to calculate the average daily gain (ADG) and feed/gain ratio (F/G). Mortality was recorded for each group.

1.13 Observation and scoring of neurological clinical symptoms

To evaluate the impact of PRV infection on mouse nervous system function and the protective effect of the drug, neurological clinical symptoms were observed and scored daily at a fixed time (9:00–10:00 AM) for each mouse[33, 34]. The specific criteria are as follows:

0 points: Normal, no neurological symptoms;

1–3 points: Mild symptoms, including ruffled fur, reduced activity, and mild tremors;

4–6 points: Moderate symptoms, including ataxia, unsteady gait, and unilateral hind limb paralysis;

7–9 points: Severe symptoms, including bilateral hindlimb paralysis, forelimb involvement, and circling;

10 points: Near death or death.

Observation commenced on day 1 postchallenge and continued until the experiment concluded (day 20). Daily scoring was recorded for each mouse, and group-average scores were calculated. Scorers were unaware of group assignments (blinded design) to ensure objectivity. Concurrently, the time of first clinical symptom onset (incubation period), time of peak symptoms, and corresponding score were recorded for each mouse.

1.14 Tissue Viral Load and Pathology Assessment

On day 14 postchallenge, three mice were randomly euthanized per group. Brain, lung, spleen, and kidney tissues were collected. An appropriate amount of tissue was weighed, homogenized in PBS, and centrifuged at 12,000 ×g for 10 minutes at 4°C to obtain the supernatant. Total DNA was extracted via the Omega Viral DNA Kit. The copy number of the PRV gE gene in each tissue sample was determined via absolute quantitative real-time polymerase chain reaction (qPCR), with the results normalized to copies per milligram of tissue or per microgram of total DNA.

Mouse brain tissue was placed in 10% neutral formalin for fixation for at least 24 hours. Following ethanol gradient dehydration, xylene clearing, and paraffin embedding, 5 μm thick sections were cut. The sections were dewaxed and rehydrated before hematoxylin and eosin (H&E) staining. Pathological changes, including changes in neuronal morphology, inflammatory cell infiltration, and perivascular space widening, were observed and evaluated under an optical microscope (Olympus BX53, Japan).

1.15 Serum and liver biochemical analysis

Blood was collected from the mice. After standing at room temperature for 30 minutes, the serum was separated by centrifugation at 4°C and 3000 ×g for 15 minutes and stored at -80°C for later use. A portion of liver tissue was weighed, added to prechilled physiological saline to prepare a 10% (w/v) tissue homogenate, and centrifuged at 4°C and 12,000 ×g for 10 minutes. The supernatant was collected for subsequent testing.

Serum alanine aminotransferase (ALT) and creatinine (CREA) levels were measured via a fully automated biochemical analyzer (Mindray BS-240, China). Serum IL-6 and IL-1β concentrations were quantified via ELISA kits according to the manufacturer's protocols. Serum samples and liver homogenate supernatants were tested with commercial kits for (1) GSH-Px activity (DTNB method), (2) SOD activity (WST-1 method), and (3) MDA content (TBA method). The liver homogenate results were normalized to the protein concentration measured via the BCA method, while the serum results were expressed per unit volume.

1.16 Statistical analysis

All in vitro experiments were independently replicated three times. The data are presented as the means ± standard deviations. Statistical analysis was performed via SPSS 27.0 software. Comparisons among multiple groups were conducted via one-way analysis of variance (ANOVA), followed by Duncan's multiple range test for significant differences. Differences in mouse survival rates were compared via the log-rank test. Differences were considered statistically significant at $P< 0.05$. All figures and tables were generated via GraphPad Prism 10.0 software.

Results

2.1 LpR Strain Fermentation Alters the Metabolomic Profile of Phellodendron amurense Aqueous Extract

To evaluate the growth-supporting effect of Phellodendron amurense aqueous extract (PAE) as a fermentation substrate for LpR (LpR), we measured viable cell concentrations before and after fermentation (0 h and 48 h) (Fig. 2A). At 0 h of fermentation, the viable cell concentration of LpR in PAEs was 2.80 ± 0.15 × 10^7 CFU/mL, which significantly increased to 7.82 ± 0.34 × 10^7 CFU/mL after 48 h of fermentation ($P< 0.05$). These results indicate that the aqueous extract of Phellodendron amurense effectively supports LpR growth and significantly promotes its proliferation. The cell biomass reached its peak after 48 h of fermentation, making it suitable for subsequent preparation of Phellodendron fermentation extract (FPAE) and metabolomic analysis.

To elucidate fermentation-induced changes in chemical composition, nontargeted metabolomics analysis was performed on fermented (FPAE) and unfermented (PAE) samples. Principal component analysis (PCA) revealed (Fig. 2B) that the metabolic profiles of the FPAE and PAE groups along the first principal component (PC1) explained 50.96% of the variance, whereas the second principal component (PC2) explained 13.87% of the variance. The two groups were completely separated in the two-dimensional space defined by PC1 and PC2, further confirming that fermentation significantly altered the metabolic profiles and indicating that the fermentation process profoundly reshaped the chemical composition of the PAE. The quality control (QC) samples clustered tightly in both positive and negative ion modes, confirming the data stability and reproducibility (Supplementary Fig. S1A). Additionally, when the PAE group was compared with the lactic acid bacteria supernatant (LpS) control group, the two groups were clearly separated on the PCA score plot (Fig. 2C). This strongly suggests that the unique chemical profile of the fermented extract likely arises not only from bacterial metabolite secretion but also from the products of biotransformation of the *Phellodendron amurense* matrix. We subsequently screened for differentially expressed metabolites via a volcano plot. With a threshold of variable importance projection (VIP) > 1 and $P< 0.05$, 2,850 significantly differentially expressed metabolites were identified in FPAE vs PAE (Fig. 2D), including 1,002 metabolites with increased levels, 537 with decreased levels, and 1,311 with no significant change. In the PAE vs LpS comparison (Fig. 2E), 1,870 differentially abundant metabolites were identified.

To systematically elucidate the chemical nature of fermentation products, we integrated multiple comparative datasets (Tables S1, S2, and S3). The results indicate that fermentation significantly altered the content of a series of key bioactive compounds. The characteristic alkaloid berberine in Phellodendron amurense increased 2.5-fold ($P< 0.05$). Concurrently, the levels of multiple phenolic acids, such as ferulic acid, and flavonoids, such as kaempferol, which are known for their antioxidant activity, significantly increased ($P< 0.05$). Notably, the ferulic acid content in FPAE was 15.2-fold greater than that in PAE ($P< 0.05$).

KEGG pathway enrichment analysis of the differentially abundant metabolites (Fig. 2F) revealed that these changes were closely associated with perturbations in specific metabolic pathways. Pathways related to plant secondary metabolites, such as “Biosynthesis of various plant secondary metabolites” and “Degradation of flavonoids”, were among the enriched categories. The significantly enriched pathways included “benzoate degradation” (rich factor = 0.56, $P = 0.033$), “phenylalanine metabolism” (rich factor = 0.42, $P = 0.042$), “degradation of flavonoids” (rich factor = 0.50, $P = 0.046$), and “biosynthesis of nucleotide sugars” (rich factor = 0.62, $P = 0.047$) (all $P< 0.05$). Further differential abundance score analysis revealed (Fig. 2G) a global reprogramming of microbial metabolic networks during fermentation: pathways associated with the utilization of Phellodendron amurense components (e.g., benzoate degradation) presented increased activity, whereas those related to bacterial basal growth and energy metabolism (e.g., glycolysis/gluconeogenesis) presented relative downregulation. This metabolic shift suggests that *L. plantarum* R may allocate more resources toward adapting to and transforming the complex plant matrix of Phellodendron amurense during fermentation. In summary, our metabolomics data revealed that *L. plantarum* R fermentation significantly altered the chemical profile of PAE, enriching certain potentially bioactive phenolic acids and flavonoids. This effect likely stems from perturbations in relevant plant secondary metabolic pathways and adaptive metabolic reprogramming within the microbial network during fermentation.

2.2 FPAE Exhibits Enhanced Anti-PRV Activity In Vitro

To systematically evaluate the impact of LpR fermentation on the PRV activity of Phellodendron water extracts, we first assessed the cytotoxicity of each sample toward PK-15 cells via the CCK-8 assay to determine safe dosing concentrations for subsequent experiments. The results of the CCK-8 assay indicated that neither FPAE nor PAE had a significant effect on PK-15 cell viability at concentrations up to 5 mg/mL (Fig. 3A). Similarly, VC showed no cytotoxicity at concentrations ≤5 μg/mL (Fig. 3B), whereas the cell survival rates decreased to 55.34% and 48.68% at 25 μg/mL and 50 μg/mL, respectively. Therefore, in subsequent experiments, 5 mg/mL FPAE, 5 mg/mL PAE, and 5 μg/mL VC were used, and the corresponding concentrations of LpS were diluted to treatment concentrations.

Validation of the PRV infection model in PK-15 cells To confirm that the PRV stock could infect PK-15 cells productively, a $TCID_{50}$ assay was performed. PK-15 cells were inoculated with serial 10-fold dilutions of the virus, and the proportion of CPE-positive wells was recorded at 72 h post-infection. As shown in Fig. 3C, the percentage of CPE-positive cells decreased in a dilution-dependent manner. The

viral titer was calculated via the Karber method to be $10^{-4.75}$ $TCID_{50}$ per 0.1 mL (the dashed line indicates the 50% endpoint). These results confirmed that the PRV stock was replication- competent and induced typical cytopathic effects, providing a reliable virus source for subsequent antiviral assays.

With this model and methodology, we systematically evaluated the effects of different treatments on the PRV load at various infection time points (24 h, 48 h, and 72 h) and concentration gradients (0.625, 1.25, 2.5, and 5 mg/mL). At 72 hpi, the viral load in the 2.5 mg/mL FPAE-treated group was only 46.77% that in the viral control group, which was significantly lower than that in the PAE group at the same concentration (P<0.05) (Fig. 3G). At 5 mg/mL, FPAE achieved an 84.15% inhibition rate against PRV, significantly outperforming PAE (63.21%) and the positive control VC (68.42%, P<0.05) (Fig. 3F). Taken together, as shown in Fig. 3F–I, these findings indicate that FPAE treatment significantly inhibited PRV replication in PK-15 cells in a concentration- and time-dependent manner.

Concentration gradient experiments demonstrated that FPAE exhibited antiviral activity across the range of 0.625–5 mg/mL, with inhibitory effects at each concentration outperforming those of PAE at corresponding concentrations. For example, the 5 mg/mL FPAE group presented a 16.20% greater inhibition rate than did the 0.625 mg/mL group at 72 hpi, indicating concentration-dependent activity. Compared with the viral control group, the LpS-treated group presented no significant difference in viral load at either 48 or 72 hours (P> 0.05). In summary, the above results suggest that the enhanced antiviral activity of FPAE primarily stems from the biotransformation of *Phellodendron amurense* components during fermentation rather than from the direct action of LpR metabolites.

2.3 FPAEs alleviate cellular oxidative damage

To investigate whether the enhanced antiviral activity of FPAE is correlated with its ability to alleviate oxidative stress, we measured the activity of antioxidant enzymes (GSH-Px, SOD) and the content of the lipid peroxidation product MDA in infected cells. As shown in Fig. 4A-C, the viral control group presented significantly decreased GSH-Px and SOD activity (P<0.05) and increased MDA levels (P<0.05) at a concentration of 2.5 mg/mL. Compared with PAE, FPAE treatment significantly increased GSH-Px and SOD activity (P<0.05) and decreased MDA levels (P<0.05) in PRV-infected cells (Fig. 4A-C). Concentration gradient experiments further confirmed that, compared with PAE, LpS, and VC at equivalent concentrations, FPAE, within the range of 0.625–5 mg/mL, had superior effects on enhancing GSH-Px/SOD activity and reducing the MDA content, with consistent trends (Fig. S2).

2.4 Establishment of a PRV infection model and safety validation of therapeutic doses

To establish a PRV infection model for in vivo efficacy evaluation, preliminary experiments were conducted to determine the optimal viral challenge dose and safe therapeutic doses. Preliminary results indicated that intramuscular inoculation with a 100-fold diluted PRV stock mixture resulted in a 37.5% survival rate in mice, which approached the median lethal dose (LD_{50}), making it suitable for subsequent efficacy evaluation (Fig. 5A). The safety of the oral administration of PAE and FPAE at different concentrations was subsequently assessed. After 7 consecutive days of oral administration of 125

mg/mL PAE or FPAE, no deaths or significant toxic reactions were observed in the mice, with a 100% survival rate. Therefore, this concentration was established as the safe dosing level for subsequent in vivo experiments (Fig. 5B-C).

2.5 Effects of FPAE on growth performance and mortality following lethal PRV challenge

To validate the in vivo antiviral efficacy of fermented FPAE, the protective effect of FPAE was evaluated in a PRV-infected mouse model (the experimental workflow is shown in Fig. 6A). As depicted in Fig. 6B, compared with the PRV model, FPAE treatment significantly increased the average daily gain (ADG) ($P<0.05$) and demonstrated superior efficacy. No statistically significant differences in average daily feed intake (ADFI) were observed among the groups ($P>0.05$) (Fig. 6C). In terms of the feed-to-gain ratio (F/G), the FPAE group presented a significantly lower F/G ($P<0.05$) than the PRV group did, indicating that FPAE effectively improved nutrient conversion under infection conditions (Fig. 6D).

Survival analysis (Fig. 6E) revealed that only the LpS and PRV model groups died during the first 12 days after challenge, with early mortality rates of 6.67% and 13.33%, respectively. No deaths occurred in the other groups during this period. From day 12 to 24, additional deaths occurred only in the PRV model group. By the end of the experiment (day 24), the overall survival rate was 80% in the FPAE-treated group, which was significantly greater than the 53.33% in the PRV model group. The PAE and VC groups both had a survival rate of 73.33%, whereas the LpR group had a survival rate of 66.67%.

With respect to neurological clinical symptoms (Fig. 6F), the PRV model group peaked symptom score of 8.5 ± 0.7. Compared with the PRV model, FPAE treatment not only delayed the onset of clinical symptoms but also significantly reduced peak severity ($P<0.05$). By the end of the experiment, all surviving FPAE-treated mice had recovered to baseline neurological scores, whereas surviving animals in the PRV and PAE groups retained varying degrees of neurological deficits.

2.6 FPAE Inhibits Viral Replication and Mitigates Pathological Damage in Target Organs

In the PRV-infected mouse model, FPAE demonstrated significant antiviral activity and organ-protective effects in vivo. The results revealed that FPAE effectively suppressed PRV replication in multiple key target organs (Fig. 7A-D). Compared with that in the PRV group, the viral load in the brain tissue was significantly lower in the FPAE group ($P<0.05$), and reductions of approximately 25–28% were also observed in the lung, spleen, and kidney tissues (all $P<0.05$). Histopathological analysis further revealed (Fig. 7E) that in the PRV model group, brain tissue exhibited extensive neuronal cell atrophy (green arrows), characterized by reduced cell body size, irregular morphology, and indistinct nuclear–cytoplasmic boundaries. Additionally, widened perivascular spaces (red arrows) were observed in the PRV model group, indicating brain edema or an inflammatory response. In contrast, the neurons in the brain tissue of FPAE-treated mice were large, rounded, and plump, with lightly stained nuclei and clearly defined boundaries (blue arrows), and the perivascular spaces appeared nearly normal. No pathological changes were observed in the tissues of the Mock group mice. These results indicate that FPAE

significantly attenuates the histopathological changes induced by PRV infection and provides effective protection in mice.

2.7 FPAE Alleviates Direct Liver Damage and Oxidative Stress Induced by PRV Infection

To evaluate the protective effect of FPAE on the livers of PRV-infected mice, serum liver injury markers and hepatic antioxidant indices were measured (Fig. 8A-B). The serum creatinine (CREA) level in the FPAE group was lower than that in the PRV group and reached a level comparable to that in the mock group; however, the difference was not statistically significant ($P>0.05$). Compared with the PRV model group, the FPAE intervention group presented significantly lower serum ALT levels ($P<0.05$), indicating its efficacy in mitigating hepatocyte injury. With respect to hepatic antioxidant capacity (Fig. 8C-E), FPAE treatment significantly increased glutathione peroxidase (GSH-Px) activity ($P<0.05$). The results also revealed trends toward decreased malondialdehyde (MDA) content and elevated superoxide dismutase (SOD) activity, although neither change reached statistical significance (both $P>0.05$). These findings indicate that FPAE effectively mitigates direct liver damage induced by PRV infection by enhancing hepatic antioxidant defense.

2.8 FPAE Improves Systemic Oxidative Stress and Inflammatory Status Induced by PRV Infection

To investigate the systemic effects of FPAE in PRV-infected mice, serum antioxidant marker and inflammatory cytokine levels were assessed. The results demonstrated that FPAE significantly ameliorated infection-induced systemic oxidative stress and suppressed inflammatory responses. Compared with the PRV treatment, the FPAE intervention significantly increased serum glutathione peroxidase (GSH-Px) activity ($P<0.05$) and tended to reduce malondialdehyde (MDA) content and increase superoxide dismutase (SOD) activity in the FPAE intervention group (Fig. 9A-C), although these changes did not reach statistical significance (both $P>0.05$). Inflammatory factor assays (Fig. 9D-E) revealed that FPAE treatment markedly reduced the serum IL-6 level ($P<0.05$) compared with that in the PRV model group, with superior efficacy compared with that in the vitamin C-positive control group. Additionally, the serum IL-1β levels in the FPAE group were lower than those in the PRV group, but the difference was not statistically significant ($P>0.05$). These findings indicate that FPAE exerts systemic protective effects by increasing antioxidant capacity and suppressing excessive inflammation.

Discussion

Phellodendron amurenseand its extracts exhibit broad-spectrum antiviral activity through direct inhibition of viral replication and induction of host antiviral states via immunomodulation. Animal studies have confirmed that its aqueous extract enhances protection against lethal influenza virus challenge[35]. In recent years, probiotic fermentation in traditional Chinese medicine (TCM) has gained significant attention. Fermenting TCM herbs with probiotics such as *Lactobacillus* and Bifidobacterium alters their chemical composition and biological activity through microbial biotransformation, offering advantages such as enhanced efficacy, reduced toxicity, and improved palatability[36]. This study is the first to systematically demonstrate the synergistic antiviral effect of LpR-fermented P. amurense extract (FPAE)

against PRV. Evidence at the “component–cell–animal” level confirms that FPAE enhances antiviral efficacy in vitro and in vivo by restructuring the active component profile, synergistically inhibiting viral replication, and regulating the oxidative-inflammatory balance.

This study revealed that Phellodendron amurense aqueous extract (PAE) significantly promoted the proliferation of LpR (LpR), with a marked increase in the viable bacterial concentration after 48 h of fermentation ($P<0.05$). This result validates the biocompatibility of Phellodendron amurense as a fermentation substrate. Although traditional Chinese medicine extracts often contain antibacterial components, such as alkaloids and phenolic acids, that may inhibit probiotic growth, the vigorous growth of LpRs in PAE indicates that PAE not only has no significant toxicity toward this strain but also provides a suitable nutritional environment. These findings provide crucial feasibility for establishing a “traditional Chinese medicine-probiotic” synergistic fermentation system.

Metabolomic analysis revealed significant regulatory effects of LpR fermentation on the active compound profile of *Phellodendron amurense*. After fermentation, multiple components with potential antiviral and antioxidant activities, including phenolic compounds (catechol, resorcinol), flavonoids (kaempferol, quercetin), and organic acids (ferulic acid, succinic acid), were significantly enriched in the bark extract, and the contents of the alkaloids berberine and berberine (berberine base) increased to 2.5 times the prefermentation level. These compositional shifts may synergistically enhance the antiviral and immunomodulatory functions of Phellodendron. Flavonoids, such as kaempferol and quercetin, have been demonstrated to directly interfere with viral replication by inhibiting the transcription of the PRV immediate-early gene *IE180* or interacting with the viral gD protein[37]. Organic acids, particularly ferulic acid, whose content increases 15-fold, are renowned for their antioxidant, anti-inflammatory, and neuroprotective properties. The synergistic action of phenolic compounds with berberine may mitigate PRV-induced tissue damage by increasing antioxidant capacity, regulating inflammatory responses, and inhibiting viral replication[38]. KEGG pathway enrichment analysis further revealed fermentation-induced metabolic networks[39]. The enrichment of benzoic acid and aminobenzoic acid degradation pathways reflects microbial adaptive metabolism of the Phellodendron amurense matrix, a process that potentially enhances drug safety by reducing toxic components.

On the basis of the aforementioned metabolomics findings, the anti-PRV activity of different treatment groups on PK-15 cells was further evaluated. The results revealed that both FPAE and PAE reduced PRV-induced cytopathic effects and viral loads in a dose-dependent manner. However, compared with PAE, FPAE exhibited significantly superior antiviral efficacy ($P<0.05$), confirming that LpR fermentation markedly enhanced Phellodendron amurense antiviral activity. The viral load in the LpS-treated group was not significantly different from that in the viral control group ($P>0.05$), indicating that the LpR extracellular secretions lack direct anti-PRV activity. In the preliminary experiment, the PRV challenge dose was diluted 100-fold; however, slight variations in the viral titer across batches may have led to a slightly lower mortality rate in the model group in the formal experiment (46.67% vs. 62.5%). Nevertheless, the overall trend remained consistent, and the experiment was still suitable for evaluating drug protective effects. This result suggests that the enhanced antiviral activity of FPAE primarily stems

from the biotransformation of Phellodendron amurense components during fermentation rather than from the direct action of probiotic metabolites. Moreover, the positive control (VC) also showed some antiviral activity against PRV in PK-15 cells, but the inhibition rate of FPAE was significantly greater than that of the PAE and VC groups. These findings indicate that fermentation significantly enhances the antiviral activity of *Phellodendron amurense* extract.

Oxidative stress is a key mechanism of cellular damage induced by PRV infection[40, 41]. This study demonstrated that PRV infection induces oxidative stress in PK-15 cells, as manifested by significantly decreased GSH-Px and SOD activities and markedly elevated MDA levels. FPAE treatment significantly reversed these changes, resulting in a dose-dependent increase in antioxidant enzyme activity and a reduction in lipid peroxidation levels across the 0.625–5 mg/mL concentration range, with superior efficacy compared with PAE at equivalent concentrations. This result suggests that enhancing the cellular antioxidant defense capacity represents a key mechanism underlying the synergistic antiviral effect of FPAE. GSH-Px and SOD are primary intracellular antioxidant enzymes whose activities reflect the cellular capacity to scavenge reactive oxygen species (ROS); MDA levels indicate the severity of oxidative damage. The ameliorative effects of FPAE on these indicators may be due to its high content of active components, such as ferulic acid and berberine. Ferulic acid has been demonstrated to directly scavenge free radicals and activate the Nrf2 antioxidant pathway[42]. The significant enrichment of these components after fermentation provides the material basis for the enhanced antioxidant effects of FPAEs. In summary, FPAE alleviates PRV-induced oxidative damage by strengthening the cellular antioxidant defense system, which may represent one of its key mechanisms of antiviral potentiation.

To establish a PRV infection model suitable for efficacy evaluation, challenge dose screening was first conducted. The results showed that intramuscular injection of a 100-fold diluted PRV stock solution resulted in a 62.5% mortality rate in mice, which approached the lethal dose (LD_{50}), making it suitable for subsequent studies. Pathological necropsy revealed typical lesions in infected mice, including cerebral edema and hemorrhage, pulmonary congestion, and intestinal distension. Viral load detection revealed the highest viral copy numbers in brain and lung tissues, confirming the strong tropism of PRV for the nervous and respiratory systems, which is consistent with previous reports[43]. For these experiments, brain tissue was selected for pathological observation, and the viral loads in the brain, lung, spleen, and kidney tissues were detected. Preliminary safety dose studies indicated that 1.25 mg/mL FPAE or PAE administered via continuous oral gavage for 7 days elicited no toxic reactions in mice, making this dosage suitable for subsequent in vivo experiments. In the PRV infection model, FPAE treatment significantly increased the mouse survival rate to 80%, outperforming both the PAE group (73.33%) and the VC group (73.33%). It also markedly improved growth performance (ADG, F/G) and neurological symptoms in infected mice ($P<0.05$). The viral load is a core indicator for evaluating antiviral efficacy and reflects pathogen replication dynamics; histopathological changes reveal the extent of infection--induced host damage and the protective efficacy of interventions at the morphological level[44, 45]. In the present study, FPAE treatment significantly suppressed PRV replication in target organs (brain, lung, spleen, and kidney), with the most pronounced reduction observed in brain tissue ($P<0.05$), resulting in approximately 25%–28% reductions in the other organs. Histopathological analysis further confirmed

that FPAE mitigated brain damage, including neuronal shrinkage. These results indicate that FPAE significantly improves survival rates and growth performance in PRV-infected mice by inhibiting viral replication and alleviating pathological damage in vivo.

The correlation between the viral load and histopathological damage has been confirmed in multiple viral infection models[46, 47]. The dual action of FPAE in suppressing viral replication and reducing pathological damage may be attributed to the synergistic regulation of oxidative stress and inflammatory responses by its fermentation-enriched components, such as berberine and ferulic acid.

PRV infection indirectly damages the liver by inducing oxidative stress and inflammatory responses. ALT is a sensitive indicator of hepatocyte injury, with elevated serum levels reflecting increased hepatocyte membrane permeability or cell necrosis[48, 49]. In this study, the PRV model group presented significantly elevated ALT levels, which is consistent with previous reports. The liver, which is rich in mitochondria and oxidative metabolic enzymes, is particularly vulnerable to oxidative stress attacks. GSH-Px and SOD are major hepatic antioxidant enzymes, whereas MDA is the end product of lipid peroxidation. Thus, GSH-Px, SOD, and MDA can serve as indicators of hepatic oxidative stress[50]. In this study, FPAE treatment significantly reduced the serum ALT level, increased the GSH-Px activity, and tended to improve the SOD and MDA levels. Previous studies have demonstrated that the activation of antioxidant signaling pathways, such as Nrf2, enhances hepatic antioxidant defense[51-54]. In line with these findings, our results suggest that FPAE may exert its hepatoprotective effects, at least in part, by activating these pathways. Notably, the hepatoprotective effects of FPAE may be indirectly related to its ability to inhibit viral replication and reduce systemic inflammation [55].

PRV infection can induce inflammatory responses in mice[56, 57]. Similarly, in this study, serum inflammatory factor analysis revealed significantly elevated IL-6 levels in the PRV model group compared with those in the blank control group. Moreover, compared with those in the PRV model group, the IL-6 levels were significantly lower in all the treatment groups, with the FPAE group exhibiting the lowest IL-6 content, which was significantly lower than those in the PAE, LpS, and VC groups ($P<0.05$). Notably, the IL-1β levels in the serum were not significantly different among the groups ($P>0.05$). Overall, previous studies have demonstrated that various fermentation products and natural compounds can inhibit these pathways, thereby reducing inflammatory responses[58]. In the present study, fermented Phellodendron amurense extract (FPAE) significantly reduced serum IL-6 levels in PRV-infected mice. Given the known anti-inflammatory properties of its enriched fermentation products (e.g., berberine and ferulic acid), it is plausible that FPAE exerts its anti-inflammatory effect through synergistic inhibition of the NF-κB/MAPK signaling pathways[35, 59, 60]. Further validation can be achieved through NLRP3 protein detection and dynamic cytokine monitoring at multiple time points.

In summary, at a dose of 892 mg/kg body weight (equivalent to 125 mg/mL oral solution, 200 μL/mouse), FPAE demonstrated good safety in PRV-infected mice, significantly suppressed viral replication in tissues such as the brain and lungs, and improved neuronal pathology and clinical damage. It alleviates oxidative stress by increasing GSH-Px activity while simultaneously suppressing the

proinflammatory cytokine IL-6, thereby reducing inflammatory responses[61]. Furthermore, this treatment significantly improved growth performance and survival rates, confirming its antiviral, metabolic regulatory, and organ-protective functions.

Several limitations of this study should be acknowledged. First, although the mouse model is widely used for initial efficacy evaluation, the natural host of PRV is swine; further validation in piglets is needed. Second, the mechanistic analysis is primarily descriptive and limited to oxidative stress and inflammatory markers; the involvement of specific signaling pathways (e.g., Nrf2 and NF-κB) remains hypothetical and requires experimental verification. Third, we did not isolate individual bioactive compounds from FPAE, so the contribution of each component to the overall antiviral effect is unclear.

Conclusion

In conclusion, this study demonstrated that LpR fermentation reconfigures the chemical composition of *Phellodendron amurense*, enriching its active components, such as berberine, ferulic acid, and kaempferol, thereby significantly enhancing its antioxidant and anti-inflammatory functions. FPAE inhibits PRV replication and alleviates oxidative stress in vitro while improving survival rates and growth performance and reducing multiorgan pathological damage in PRV-infected mice in vivo. FPAE protects systemic health by regulating GSH-Px antioxidant enzyme activity and the levels of the inflammatory factor IL-6 (Fig. 10). This study provides a theoretical basis for the development of probiotic-fermented plant-based feed additives to control PRV infection in swine.

Declarations

Acknowledgments The authors thank the College of Veterinary Medicine, Henan Agricultural University for providing laboratory facilities. We are grateful to the staff of the Henan Provincial Laboratory Animal Center for their assistance with animal care.

Author contributions Mengyao Zhao: data curation, investigation, methodology, writing – original draft. Feifan Wu: data curation, investigation, methodology, writing – original draft. Zenghao Xu: data curation. Xing Han: investigation. Sai Mao: investigation. Hongying Zhang: methodology. Yina Zhang: conceptualization, project administration, funding acquisition, writing – review and editing. Mingfan Yang: conceptualization, project administration, funding acquisition, writing – review and editing.

Funding This research was funded by the National Natural Science Foundation of China (Grant No. 32302890), the Natural Science Foundation of Henan Province (Grant No. 262300421131), and the Natural Science Foundation of Henan Province for Young Scientists (Grant No. 252300421660).

Data availability Data from this study are available to readers upon reasonable request.

Ethics statement All animal experimental procedures were approved by the Animal Care and Use Committee of Henan Agricultural University (Approval NoHNND2024030728, approved on March 7,

2024). All experiments were performed in accordance with the guidelines for the care and use of laboratory animals.

Competing interests The authors declare no competing interests.

References

1. Hu T, Gao S, Yu Z, Liu Y, Tang H, Xu Z, Zhu L, Zhao L, Ye G, Shi F (2025) Rosmarinic acid inhibits pseudorabies virus (PRV) infection by activating the cGAS-STING signaling pathway. BMC Microbiol. 25(1):149. https://doi.org/10.1186/s12866-024-03732-4
2. Zheng H H, Fu P F, Chen H Y, Wang Z Y (2022) Pseudorabies virus: From pathogenesis to prevention strategies. Viruses. https://doi.org/10.3390/v14081638
3. Serena M S, Cappuccio J, Fossaroli M, Williman M M, Dibarbora M, Brizzio R, Metz G E, Aspitia C G, Perez A, Carpinetti B N, Echeverría M G (2023) Characterization of new strains of pseudorabies virus in Argentina: Detection of interspecies transmission. Open Vet J. 13(4):419–426. https://doi.org/10.5455/OVJ.2023.v13.i4.3
4. Wang G, Zha Z, Huang P, Sun H, Huang Y, He M, Chen T, Lin L, Chen Z, Kong Z, Que Y, Li T, Gu Y, Yu H, Zhang J, Zheng Q, Chen Y, Li S, Xia N (2022) Structures of pseudorabies virus capsids. Nat Commun. 13(1):1533. https://doi.org/10.1038/s41467-022-29250-3
5. Chen X, Yu Z (2024) Insight into the interaction mechanism of pseudorabies virus infection. Biology (Basel). https://doi.org/10.3390/biology13121013
6. Ren Q, Ren H, Gu J, Wang J, Jiang L, Gao S (2022) The epidemiological analysis of pseudorabies virus and pathogenicity of the variant strain in Shandong Province. Front Vet Sci. https://doi.org/10.3389/fvets.2022.806824
7. Sun Y, Zhao L, Fu Z F (2022) Effective cross-protection of a lyophilized live gE/gI/TK-deleted pseudorabies virus (PRV) vaccine against classical and variant PRV challenges. Vet Microbiol. 267(109387. https://doi.org/10.1016/j.vetmic.2022.109387
8. Song C, Ye H, Zhang X, Zhang Y, Li Y, Yao J, Gao L, Wang S, Yu Y, Shu X (2024) Isolation and characterization of Yunnan variants of the pseudorabies virus and their pathogenicity in rats. Viruses. https://doi.org/10.3390/v16020233
9. de Oliveira J R, Antunes B S, do Nascimento G O, Kawall J C S, Oliveira J V B, Silva K, Costa M A T, Oliveira C R (2022) Antiviral activity of medicinal plant-derived products against SARS-CoV-2. Exp Biol Med (Maywood). 247(20):1797–1809. https://doi.org/10.1177/15353702221108915
10. Bello-Onaghise G, Wang G, Han X, Nsabimana E, Cui W, Yu F, Zhang Y, Wang L, Li Z, Cai X, Li Y (2020) Antiviral strategies of Chinese herbal medicine against PRRSV infection. Front Microbiol. https://doi.org/10.3389/fmicb.2020.01756
11. Meunier T, Desmarets L, Bordage S, Bamba M, Hervouet K, Rouillé Y, François N, Decossas M, Sencio V, Trottein F, Tra Bi F H, Lambert O, Dubuisson J, Belouzard S, Sahpaz S, Séron K (2022) A photoactivable natural product with broad antiviral activity against enveloped viruses, including

highly pathogenic coronaviruses. Antimicrob Agents Chemother. 66(2):e0158121. https://doi.org/10.1128/aac.01581-21

12. Cho W K, Choi H J, Ma J Y (2025) Antiviral activity of berbamine against influenza A virus infection. Int J Mol Sci. https://doi.org/10.3390/ijms26062819
13. Huo H, Bao H, Li J, Li H (2025) Optimization and antioxidant evaluation of clean and efficient recovery of polyphenols from *Phellodendron amurense* waste leaves via ultrasound-assisted extraction. Ultrason Sonochem. https://doi.org/10.1016/j.ultsonch.2025.107512
14. Sun Y, Lenon G B, Yang A W H (2019) Phellodendri cortex: a phytochemical, pharmacological, and pharmacokinetic review. Evid Based Complement Alternat Med. https://doi.org/10.1155/2019/7621929
15. Tang L, Huang L, Lai Y (2022) Network pharmacology and bioinformatics analyses identify the intersection genes and mechanism of Huang Bai for recurrent aphthous stomatitis. Int J Immunopathol Pharmacol. https://doi.org/10.1177/03946320221129134
16. Jiao Y, Yang R (2025) Berberine alleviates respiratory syncytial virus (rsv)-induced pediatric bronchiolitis and fibrosis by suppressing the HMGB1/TLR4/NF-κB pathway. Microbiol Spectr. 13(8):e0090025. https://doi.org/10.1128/spectrum.00900-25
17. Kang H G, Wei M L, Wang J L, Ma C P, Zhang X, Huang B W, Xin L S, Bai C M (2025) Berberine, a natural compound that demonstrates antiviral effects against ostreid herpesvirus 1 infection in *Anadara broughtonii*. Viruses. https://doi.org/10.3390/v17020282
18. Chin L W, Cheng Y W, Lin S S, Lai Y Y, Lin L Y, Chou M Y, Chou M C, Yang C C (2010) Anti-herpes simplex virus effects of berberine from Coptidis Rhizoma, a major component of a Chinese herbal medicine, ching-wei-san. Arch Virol. 155(12):1933–1941. https://doi.org/10.1007/s00705-010-0779-9
19. Murakami T, Bodor E, Bodor N (2023) Approaching strategy to increase the oral bioavailability of berberine, a quaternary ammonium isoquinoline alkaloid: Part 1. Physicochemical and pharmacokinetic properties. Expert Opin Drug Metab Toxicol. 19(3):129–137. https://doi.org/10.1080/17425255.2023.2203857
20. Kohli K, Mujtaba A, Malik R, Amin S, Alam M S, Ali A, Barkat M A, Ansari M J (2021) Development of natural polysaccharide-based nanoparticles of berberine to enhance oral bioavailability: Formulation, optimization, ex vivo, and in vivo assessment. Polymers (Basel). https://doi.org/10.3390/polym13213833
21. Wang Y, Xu Q, Shen Z, Wang Y, Dong L, Fu S, Yang L, Qin M, Zhang Y, Guo S (2019) Simultaneous determination of eight active compounds in baitouweng decoction and its single herbs. J Chromatogr Sci. 57(6):502–510. https://doi.org/10.1093/chromsci/bmz022
22. Dissanayake I H, Tabassum W, Alsherbiny M, Chang D, Li C G, Bhuyan D J (2025) Lactic acid bacterial fermentation as a biotransformation strategy to enhance the bioavailability of phenolic antioxidants in fruits and vegetables: A comprehensive review. Food Res Int. https://doi.org/10.1016/j.foodres.2025.116283

23. Yang H Y, Han L, Lin Y Q, Li T, Wei Y, Zhao L H, Tong X L (2023) Probiotic fermentation of herbal medicine: progress, challenges, and opportunities. Am J Chin Med. 51(5):1105-1126. https://doi.org/10.1142/s0192415x23500519
24. Bai J, Zhu Z, Luo W, Jang M, Pan B, Zhu Y, Zhang J, Zhao Y, Xiao X (2025) Microbial fermentation affects the structure-activity relationship of bioactive compounds in ginseng and its applications in fermentation products: A review. Foods. https://doi.org/10.3390/foods14142473
25. Feng C, Wu Y, Cai Z, Song Z, Shim Y Y, Reaney M J T, Wang Y, Zhang N (2024) A comparative study on flaxseed lignan biotransformation through resting cell catalysis and microbial fermentation by β-glucosidase-producing *Lactiplantibacillus plantarum*. J Sci Food Agric. 104(10):5869–5881. https://doi.org/10.1002/jsfa.13412
26. Macedo G A, Caria C, Barbosa P P M, Mazine M R, Gambero A (2023) Bioaccessibility evaluation of soymilk isoflavones with biotransformation processing. Foods. https://doi.org/10.3390/foods12183401
27. Li Y, Liu H, Qi H, Tang W, Zhang C, Liu Z, Liu Y, Wei X, Kong Z, Jia S, Du B, Yuan J, Wang C, Li M (2021) Probiotic fermentation of *Ganoderma lucidum* fruiting body extracts promoted its immunostimulatory activity in mice with dexamethasone-induced immunosuppression. Biomed Pharmacother. https://doi.org/10.1016/j.biopha.2021.111909
28. Duan W, Guan Q, Zhang H L, Wang F Z, Lu R, Li D M, Geng Y, Xu Z H (2023) Improving flavor, bioactivity, and changing metabolic profiles of goji juice by selected lactic acid bacteria fermentation. Food Chem. https://doi.org/10.1016/j.foodchem.2022.135155
29. Zhang R, Cen Q, Hu W, Chen H, Hui F, Li J, Zeng X, Qin L (2024) Metabolite profiling, antioxidant and anti-glycemic activities of tartary buckwheat processed by solid-state fermentation (SSF) with *Ganoderma lucidum*. Food Chem X. https://doi.org/10.1016/j.fochx.2024.101376
30. Feng Y, Chen A, Chen K, Zeng L, Ran X (2026) Effects of solid-state fermentation by Eurotium cristatum on the metabolic profile of Angelica dahurica. Foods. https://doi.org/10.3390/foods15071238
31. Wang H, Teng J, Huang L, Wei B, Xia N (2023) Determination of the variations in the metabolic profile and sensory quality of liupao tea during fermentation through UHPLC-HR-MS metabolomics. Food Chem. https://doi.org/10.1016/j.foodchem.2022.134773
32. Pala E E, Pala H G, Ekmekci S, Erbas O (2022) Vitamin C (ascorbic acid) protects from neuropathy caused by cisplatin, through enhanced heat shock protein-70 and reduced oxidant effect. Rev Assoc Med Bras (1992). 68(8):1017–1022. https://doi.org/10.1590/1806-9282.20220032
33. Kim J H, Weeratunga P, Kim M S, Nikapitiya C, Lee B H, Uddin M B, Kim T H, Yoon J E, Park C, Ma J Y, Kim H, Lee J S (2016) Inhibitory effects of an aqueous extract from Cortex Phellodendri on the growth and replication of broad-spectrum of viruses in vitro and in vivo. BMC Complement Altern Med. https://doi.org/10.1186/s12906-016-1206-x
34. Guo X, Yan Z, Wang J, Fan X, Kang J, Niu R, Sun Z (2022) Effect of traditional Chinese medicine (TCM) and its fermentation using *Lactobacillus plantarum* on ceftriaxone sodium-induced

dysbacteriotic diarrhea in mice. Chin Med. 17(1):20. https://doi.org/10.1186/s13020-022-00575-x

35. Wang W, Zu Y, Fu Y, Reichling J, Suschke U, Nokemper S, Zhang Y (2009) In vitro antioxidant, antimicrobial and anti-herpes simplex virus type 1 activity of *Phellodendron amurense* Rupr. From China. Am J Chin Med. 37(1):195–203. https://doi.org/10.1142/s0192415x09006655
36. Xiao R, Wang L, Tang Z, Qian X, Wang J, Lian Y, Tang J, Xu J, Lin Y, Shi B, Xu P, Xiong Q (2024) Effects of fermented Chinese herbal medicine feed additives on growth performance and intestinal microbiota of piglets. PLoS One. https://doi.org/10.1371/journal.pone.0308196
37. Li L, Wang R, Hu H, Chen X, Yin Z, Liang X, He C, Yin L, Ye G, Zou Y, Yue G, Tang H, Jia R, Song X (2021) The antiviral activity of kaempferol against pseudorabies virus in mice. BMC Vet Res. 17(1):247. https://doi.org/10.1186/s12917-021-02953-3
38. Heidarzadeh M, Amininasab M, Rezayat S M, Mousavi S E (2024) Investigation of antioxidant and anti-inflammatory properties of berberine nanomicelles: in vitro and in vivo studies. Curr Drug Deliv. 21(9):1273–1283. https://doi.org/10.2174/0115672018258030230920035222
39. Intasian P, Sutthaphirom C, Bodeit O, Trisrivirat D, Kimprasoot N, Jaroensuk J, Bakker B, Klipp E, Chaiyen P (2024) Enhancement of essential cofactors for in vivo biocatalysis. Faraday Discuss. 252:157–173. https://doi.org/10.1039/d4fd00013g
40. Zhao Y, Qi X, Zhu Z, Wang W, Wen W, Li X (2025) Increased ROS levels activate AMPK-ULK1-mediated mitophagy to promote pseudorabies virus replication. Vet Res. 56(1):156. https://doi.org/10.1186/s13567-025-01595-9
41. Lai I H, Chang C D, Shih W L (2019) Apoptosis induction by pseudorabies virus via oxidative stress and subsequent DNA damage signaling. Intervirology. 62(3-4):116–123. https://doi.org/10.1159/000502047
42. Kose T, Moreno-Fernandez J, Vera-Aviles M, Sharp P A, Latunde-Dada G O (2023) Ferulic acid protects HepG2 cells and mouse liver from iron-induced damage. Biochem Biophys Rep. https://doi.org/10.1016/j.bbrep.2023.101521
43. Wu H, Qi H, Wang B, Li M, Qu L, Li S, Luo Y, Li L F, Zheng G L, Qiu H J, Sun Y (2023) The mutations on the envelope glycoprotein d contribute to the enhanced neurotropism of the pseudorabies virus variant. J Biol Chem. https://doi.org/10.1016/j.jbc.2023.105347
44. Li J, Zhao D, Yan S, Qiu L, Qin H, Gao X, Jiang B, Yu W, Zhu Y, Tao Y, Zhang K, Li S (2026) Antiviral effect of chelerythrine chloride against tick-borne encephalitis virus. Virol J. https://doi.org/10.1186/s12985-026-03125-1
45. Bramante C T, Beckman K B, Mehta T, Karger A B, Odde D J, Tignanelli C J, Buse J B, Johnson D M, Watson R H B, Daniel J J, Liebovitz D M, Nicklas J M, Cohen K, Puskarich M A, Belani H K, Siegel L K, Klatt N R, Anderson B, Hartman K M, Rao V, Hagen A A, Patel B, Fenno S L, Avula N, Reddy N V, Erickson S M, Fricton R D, Lee S, Griffiths G, Pullen M F, Thompson J L, Sherwood N E, Murray T A, Rose M R, Boulware D R, Huling J D (2024) Favorable antiviral effect of metformin on SARS-CoV-2 viral load in a randomized, placebo-controlled clinical trial of COVID-19. Clin Infect Dis. 79(2):354–363. https://doi.org/10.1093/cid/ciae159

46. de Sousa R M P, Garcia L S, Lemos F S, de Campos V S, Machado Ferreira E, de Almeida N A A, Maron-Gutierrez T, de Souza E M, de Paula V S (2024) CRISPR/Cas9 eye drop HSV-1 treatment reduces brain viral load: a novel application to prevent neuronal damage. Pathogens. https://doi.org/10.3390/pathogens13121087
47. Smith M D, Seleme M C, Marquez-Lago T, Chen J W, Mach M, Britt W J (2025) Early control of cochlear viral load limits cochlear inflammation and prevents virus-induced sensorineural hearing loss. J Neuroinflammation. 22(1):92. https://doi.org/10.1186/s12974-025-03416-4
48. Smith A K, Ropella G E P, McGill M R, Krishnan P, Dutta L, Kennedy R C, Jaeschke H, Hunt C A (2020) Contrasting model mechanisms of alanine aminotransferase (alt) release from damaged and necrotic hepatocytes as an example of general biomarker mechanisms. PLoS Comput Biol. https://doi.org/10.1371/journal.pcbi.1007622
49. Ren C Z, Hu W Y, Zhang J W, Wei Y Y, Yu M L, Hu T J (2021) Establishment of inflammatory model induced by pseudorabies virus infection in mice. J Vet Sci. https://doi.org/10.4142/jvs.2021.22.e20
50. Coelho Ferraz A, Bueno da Silva Menegatto M, Lameira Souza Lima R, Samuel Ola-Olub O, Caldeira Costa D, Carlos de Magalhães J, Maurício Rezende I, Desiree LaBeaud A, T P M, Augusto Alves P, Teixeira de Carvalho A, Assis Martins-Filho O, B P D, Magalhães C L B (2024) Yellow fever virus infection in human hepatocyte cells triggers an imbalance in redox homeostasis with increased reactive oxygen species production, oxidative stress, and decreased antioxidant enzymes. Free Radic Biol Med. 213(266–273). https://doi.org/10.1016/j.freeradbiomed.2024.01.042
51. Qu H, Liu S, Cheng C, Zhao H, Gao X, Wang Z, Yi J (2020) Hepatoprotection of pine nut polysaccharide via Nrf2/ARE/MKP1/JNK signaling pathways against carbon tetrachloride-induced liver injury in mice. Food Chem Toxicol. https://doi.org/10.1016/j.fct.2020.111490
52. Sun M F, Song J X, Tang M, Yu B H, Xiao Y, Gao Y H, Yao Z X, An K Y, Zhang Z Q, Shen Y Q, Zhao Y S (2026) Hydrogen mitigated doxorubicin-induced liver injury via Nrf2/HO-1 pathway activation. Int J Mol Sci. https://doi.org/10.3390/ijms27062774
53. Yu S, Yang N, Li H, Hu X, Zhang L, Li S (2024) Artemether ameliorates acetaminophen-induced liver injury through Nrf2 pathway. Biomed Pharmacother. https://doi.org/10.1016/j.biopha.2024.117280
54. Gao J, Lu W, Xin Y, Ma H, Sheng X, Gao G, Kang X, Jiang S, Zhao Y, Lv Y, Niu Y, Liang Y, Wang H (2025) Liver-specific BCL3 knockout alleviates acetaminophen-induced liver injury by activating Nrf2 pathway in male mice. Cell Mol Gastroenterol Hepatol. https://doi.org/10.1016/j.jcmgh.2025.101483
55. Zhang Q, Li N, Ma X, Qiu Y, Li C, Chen Y (2025) Berberine protects against gefitinib-induced liver injury by inhibiting the HMGB1/TLR4/NF-κB pathway. Front Pharmacol. https://doi.org/10.3389/fphar.2025.1645634
56. Tang D, Chen X, Kang R, Kroemer G (2021) Ferroptosis: Molecular mechanisms and health implications. Cell Res. 31(2):107–125. https://doi.org/10.1038/s41422-020-00441-1
57. Laval K, Vernejoul J B, Van Cleemput J, Koyuncu O O, Enquist L W (2018) Virulent pseudorabies virus infection induces a specific and lethal systemic inflammatory response in mice. J Virol.

https://doi.org/10.1128/jvi.01614-18

58. Zhang Y, Wu N, Yin X, Piao Y, Gao M, Piao J, Li X, Zhang C, Jin L (2026) Bioactive compounds from A. Dahurica attenuate LPS-induced inflammation via dual inhibition of MAPK and NF-κB signaling pathways. J Ethnopharmacol. https://doi.org/10.1016/j.jep.2026.121361
59. Liang W T, Li J J, Lv Z R, Chen Z H, Yang Y D, Xie T Y, Ruan Y J, Tu X P, Zeng F F, Wei S, Yang X, Zhang F X (2026) *Fici hirtae radix* alleviates influenza A virus-induced acute lung injury via tlr4-pi3k-akt/p38 mapk-NF-κB signaling pathway. J Ethnopharmacol. https://doi.org/10.1016/j.jep.2025.120522
60. Hu K, Ge G, Wu B, Yang J, Ren J, Zhang L (2026) Lupiwighteone exerts anti-aging effects by suppressing NF-κB and activating the MAPKs/Nrf2 signaling pathway. Comp Biochem Physiol C Toxicol Pharmacol. https://doi.org/10.1016/j.cbpc.2026.110458
61. Zhu Z, Turak A, Xu N, Jenis J, Aisa H A (2025) Three new monoterpenes compounds isolated from Seriphidium terrae-albae exerted anti-inflammatory effects through the JAK/STAT and NF-κB signaling pathways. Fitoterapia. https://doi.org/10.1016/j.fitote.2024.106335

Figures

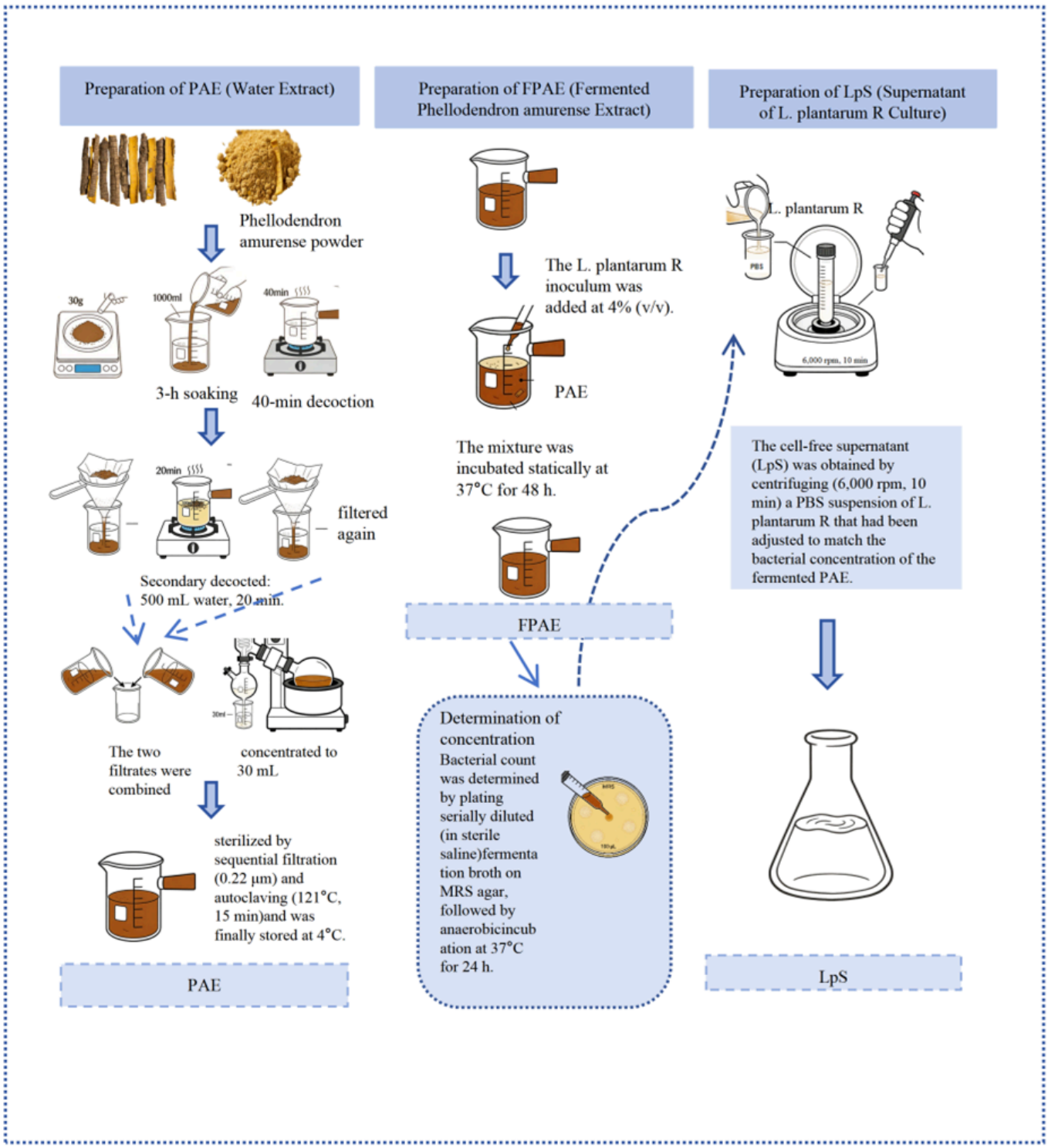

Figure 1

Schematic diagram illustrating the preparation procedures of Phellodendron amurense extract (PAE), fermented PAE (FPAE), and *Lactobacillus plantarum* R supernatant (LpS).

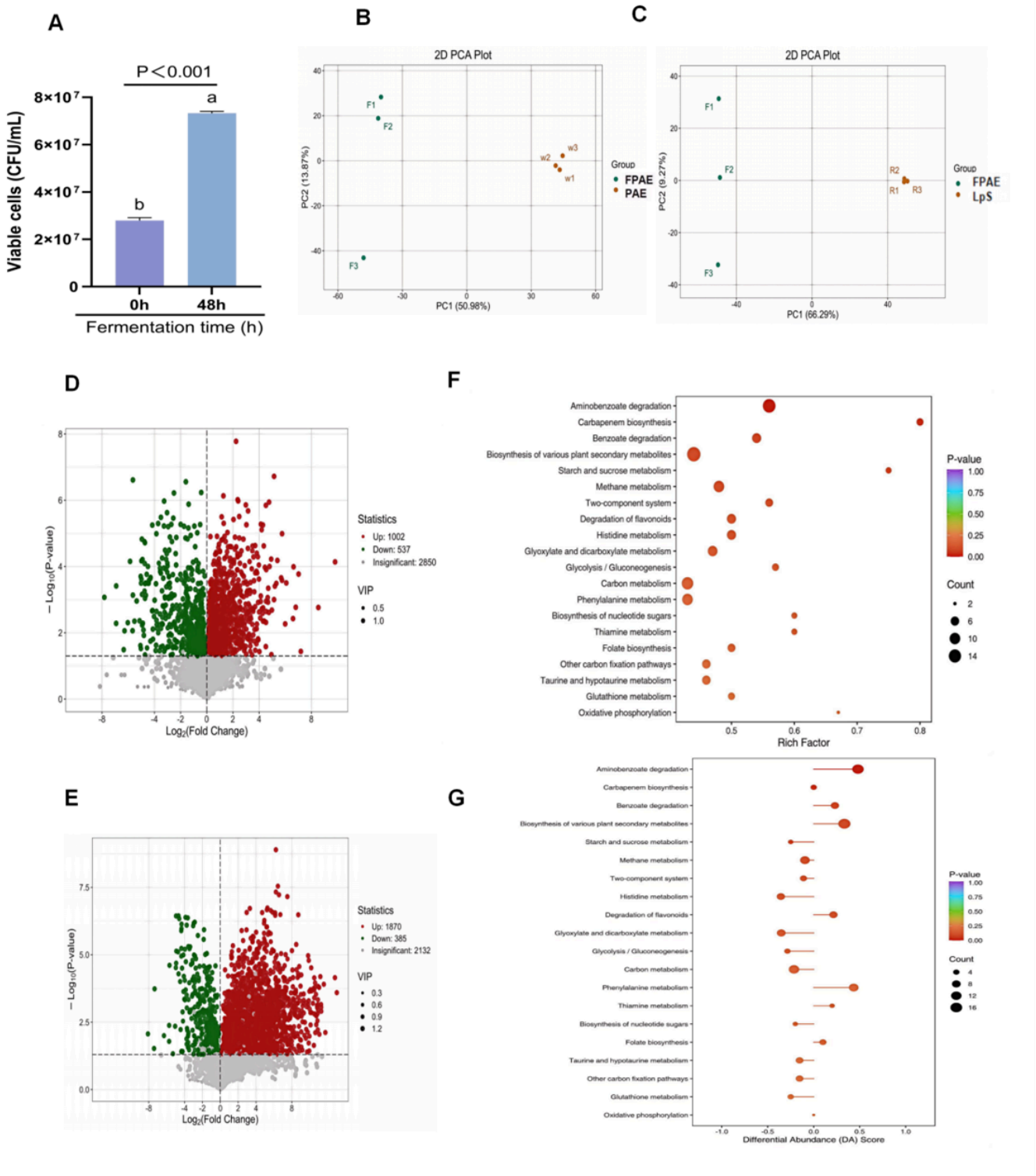

Figure 2

Metabolomic analysis of *Lactobacillus plantarum* R before and after fermentation of Phellodendron bark water extract. **(A)** viable cell counts of LpR fermenting Phellodendron bark water extract PAE at 0 h and 48 h. Different lowercase letters (a, b, c...) indicate significant differences between groups ($P<0.05$), while identical letters or no letter indicate no significant difference ($P>0.05$). **(B)** Principal Component Analysis (PCA) score plot (FPAE vs PAE). **(C)** PCA score plot (FPAE vs. LpS). **(D)** Volcano plot of

differentially abundant metabolites comparing FPAE and PAE. Red dots indicate significantly upregulated metabolites (VIP > 1, $P < 0.05$, n = 1002); blue dots indicate significantly downregulated metabolites (n = 537); gray dots indicate metabolites without significant differences (n = 2850). Dot size represents VIP value. **(E)** Volcano plot of differentially abundant metabolites (FPAE vs. LpS). **(F)** KEGG pathway enrichment plot for differentially expressed metabolites between samples (FPAE vs. PAE). Shows the top 20 most enriched pathways. Bubble size represents the number of metabolites enriched in that pathway; color indicates p value (red: smaller p value, blue: larger p value). **(G)** KEGG differential abundance score plot for differentially expressed metabolites between samples (FPAE vs. PAE).

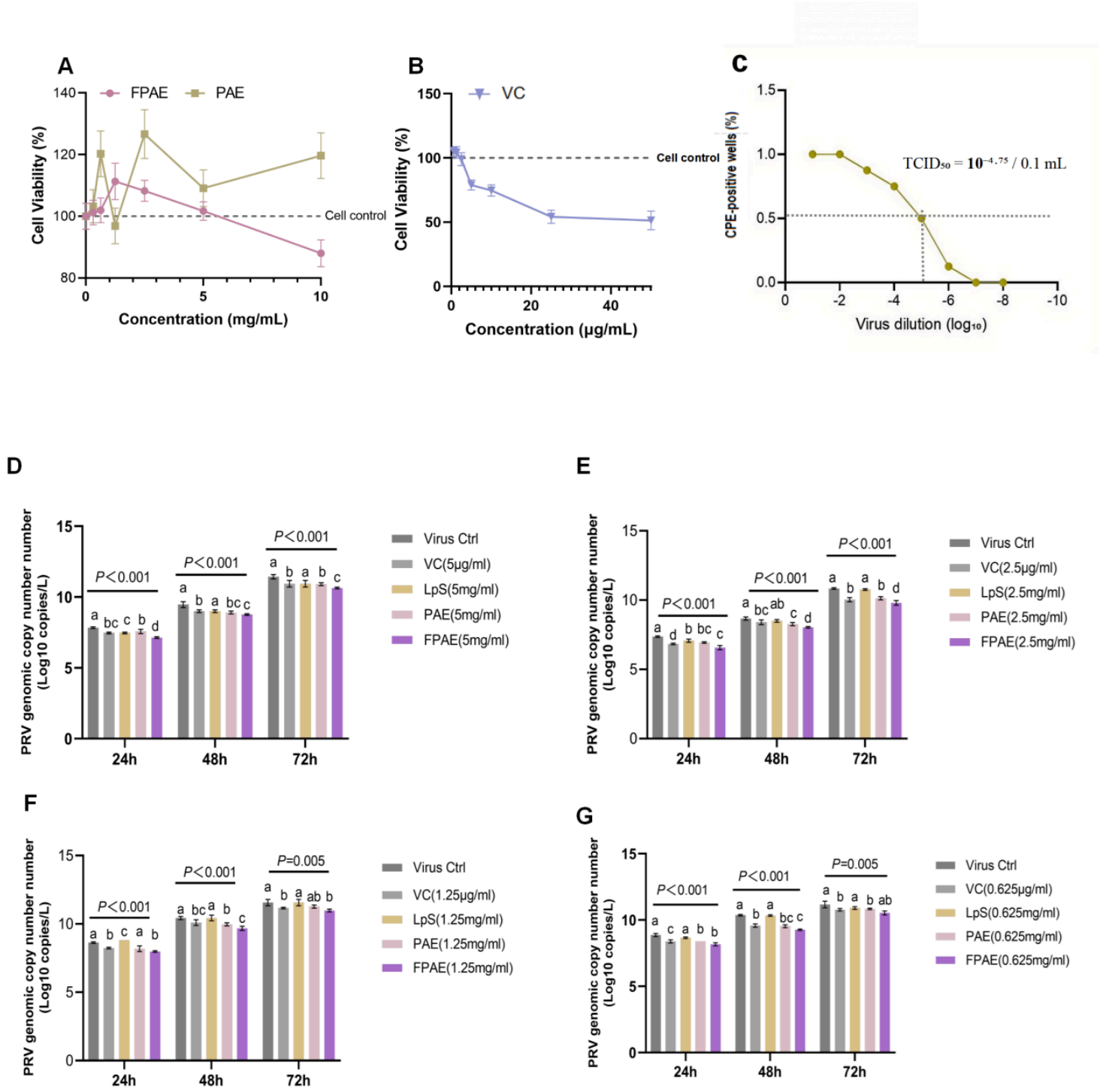

Figure 3

Antiviral activity of FPAE against pseudorabies virus (PRV) in PK-15 cells. **(A)** Cytotoxicity of FPAE and PAE to PK-15 cells. Data are mean ± SD (n=5). Dashed line: 100% viability threshold. **(B)** Cell viability of PK-15 cells after 24 h treatment with different concentrations of VC (0.625–50 μg/mL). **(C)** $TCID_{50}$ assay results for PRV in PK-15 cells (calculated using the Reed-Muench method, titer: $10^{4.75}$/0.1 mL)**.(D–F)**Effects of different treatments on PRV replication. PK-15 cells were infected with PRV (100 $TCID_{50}$)

after 4 h of sample pretreatment. Cells were harvested at 24, 48, and 72 h postinfection, and viral genome copy numbers were detected by qPCR. Data are expressed as the mean ± SEM (n=3). Different lowercase letters (a, b, c...) indicate significant differences between groups ($P<0.05$), while identical letters or no letter indicate no significant difference ($P>0.05$).

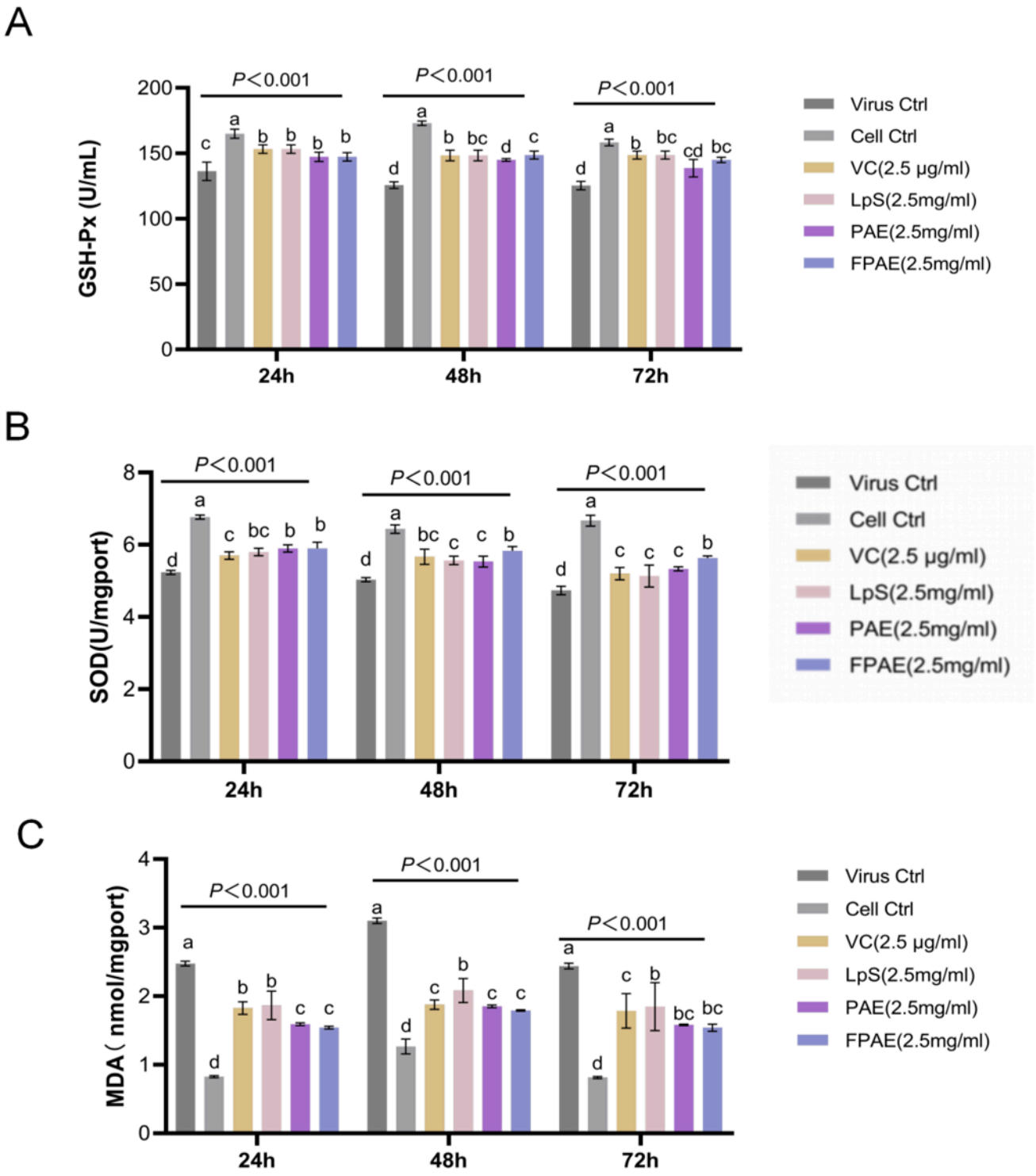

Figure 4

Mitigating effects of FPAE on Oxidative Stress in PRV-Infected PK-15 Cells **(A)** Glutathione peroxidase (GSH-Px) activity, **(B)**Superoxide dismutase (SOD) activity, and **(C)** Malondialdehyde (MDA) content data are presented as the mean ± SEM (n=3). Different lowercase letters (a, b, c...) indicate significant differences between groups (*P*<0.05).

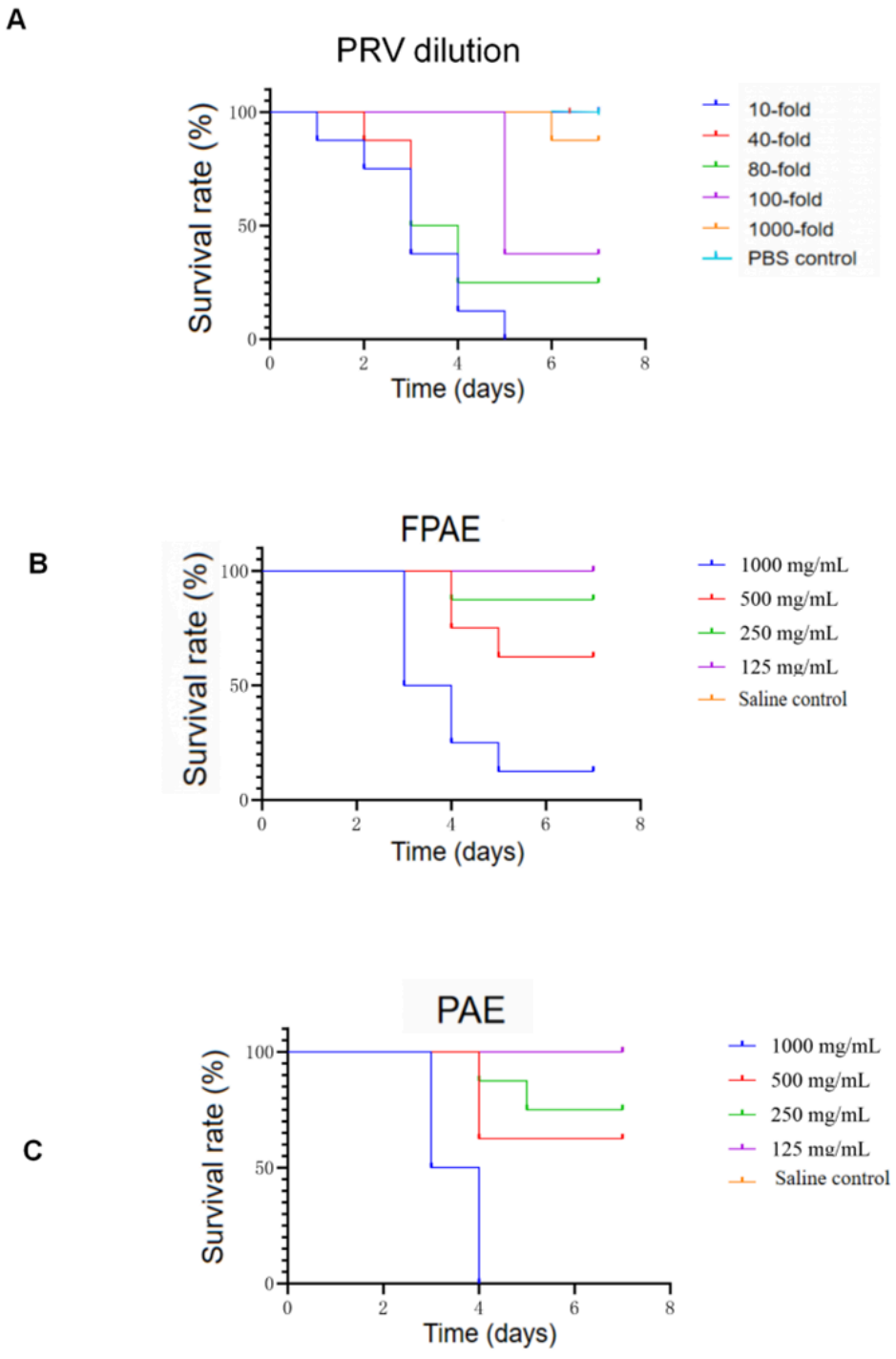

Figure 5

Establishment of a lethal PRV infection model and safety validation of Phellodendron bark extract treatment doses. **(A)** Survival rates of mice after challenge with PRV at different dilution levels. Mice (n = 8) in each group received intramuscular injections of PRV virus solutions diluted 10-, 40-, 80-, 100-, or 1000-fold, or PBS (blank control), with survival monitored continuously for 7 days. **(B–C)** Safety evaluation of oral administration of different concentrations of **(B)** Phellodendron bark aqueous extract (PAE) and **(C)** Phellodendron bark fermented extract (FPAE).content data are presented as the mean ± SEM . Different lowercase letters (a, b, c...) indicate significant differences between groups (*P*<0.05).

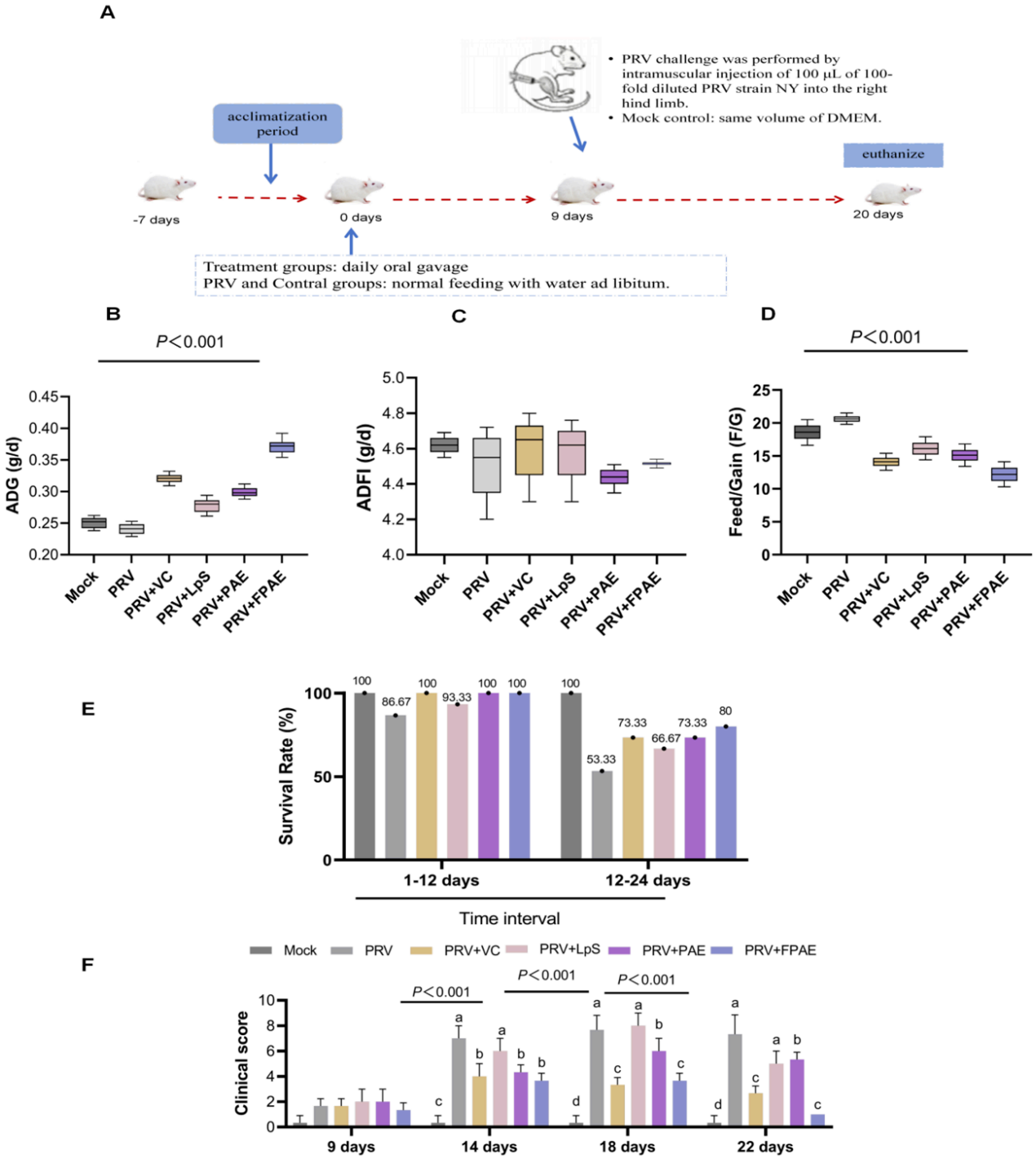

Figure 6

Protective Effect of FPAE on PRV-Infected Mice **(A)** Experimental workflow diagram. **(B)** Average daily gain (ADG) of mice in each group. n=15 **(C)** Average daily feed intake (ADFI) of mice in each group **(D)**Feed-to-gain ratio (F/G) of mice in each group **(E)** Survival rate of mice in each group **(F)** Clinical scores of mice in each group Clinical symptoms observed and recorded daily: 0 points: Normal 1–3 points: Mild symptoms (ruffled fur, mild lethargy) 4–6 points: Moderate symptoms (arched back, reduced activity) 7–9 points: severe symptoms (tremors, paralysis); 10 points: near-death or death. Data are expressed as the mean ± SEM（n=3）. Different lowercase letters (a, b, c...) indicate significant intergroup differences ($P < 0.05$); identical letters or no letters indicate no significant difference ($P > 0.05$).

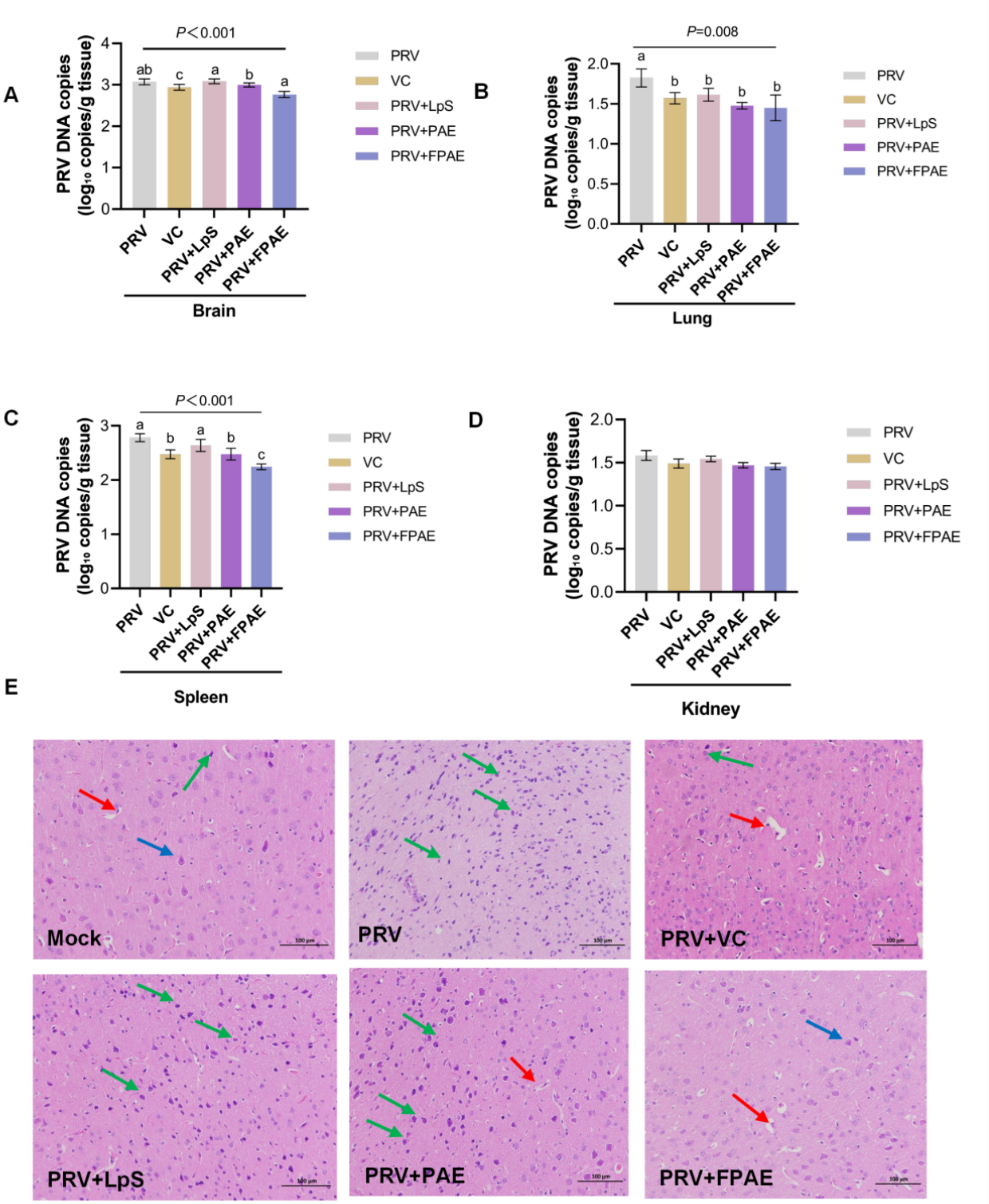

Figure 7

Effects of different treatment regimens on viral load in tissues of PRV-challenged mice. (A) Brain, (B) Spleen, (C) Lung, (D) Kidney. **(E)** Brain tissue HE staining results; Scale bar = 100 μm. Blue arrow: Normal neurons; Green arrow: Shrunken neurons; Red arrow: Widened perivascular spaces.Data are expressed as the mean ± SEM (n=3). Different lowercase letters (a, b, c...) indicate significant intergroup differences ($P< 0.05$). Identical letters or no letter indicate no significant difference ($P> 0.05$).

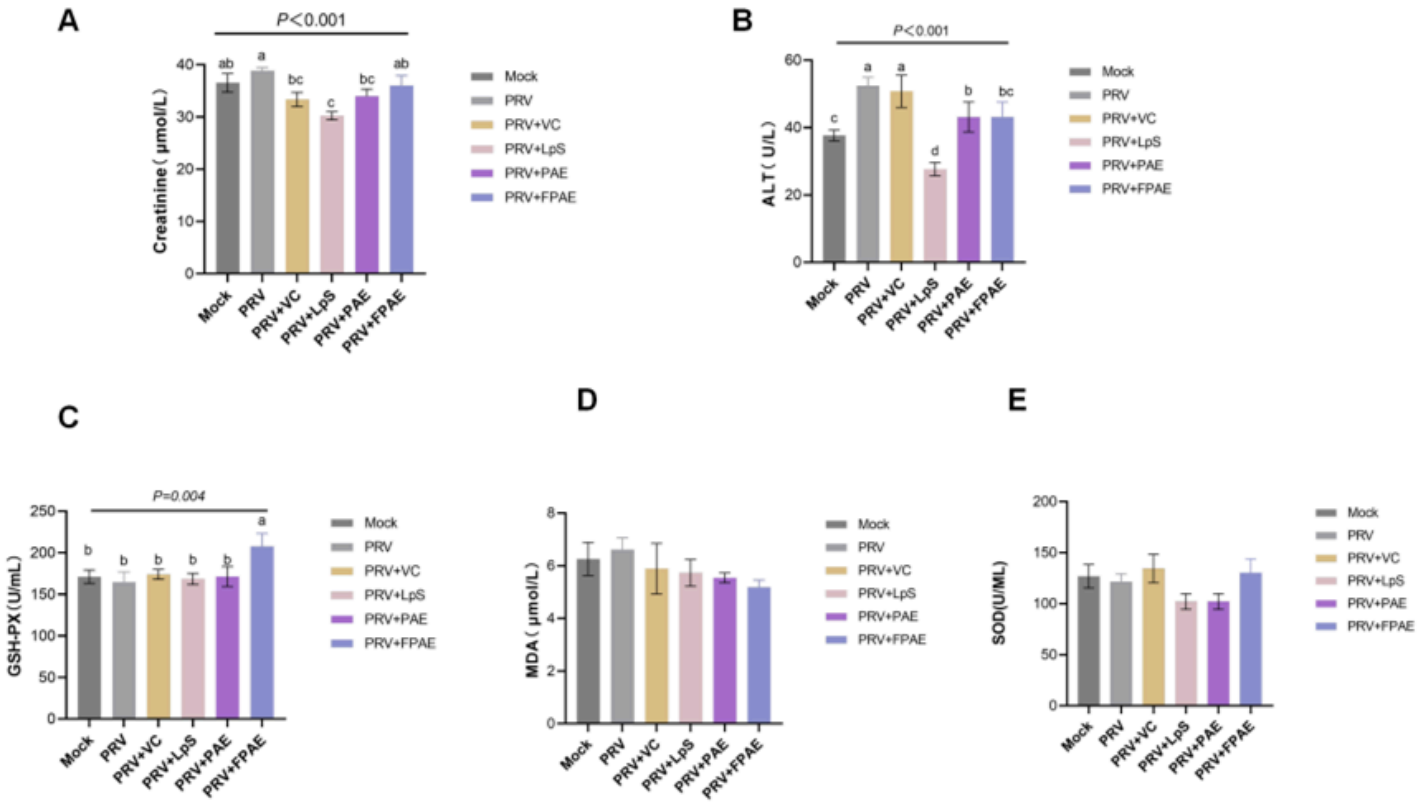

Figure 8

Effects of Different Treatment Regimens on Serum Biochemical Parameters and Liver Antioxidant Capacity in PRV-Infected Mice **(A–B)** Serum Biochemical Parameters. **(A)** Alanine aminotransferase (ALT) activity; **(B)** Creatinine (CREA) content. Data are expressed as the mean ± SEM (n=3). Different letters indicate significant intergroup differences (P< 0.05, two-way ANOVA, Tukey's post hoc test). **(C–E)** Liver tissue antioxidant parameters. **(C)** Glutathione peroxidase (GSH-Px) activity; (D) Malondialdehyde (MDA) content; **(E)** Superoxide dismutase (SOD) activity. Data are presented as the mean ± SEM (n=3). Different lowercase letters (a, b, c...) indicate significant differences between groups (P<0.05), while identical letters or no letter indicate no significant difference (P>0.05).

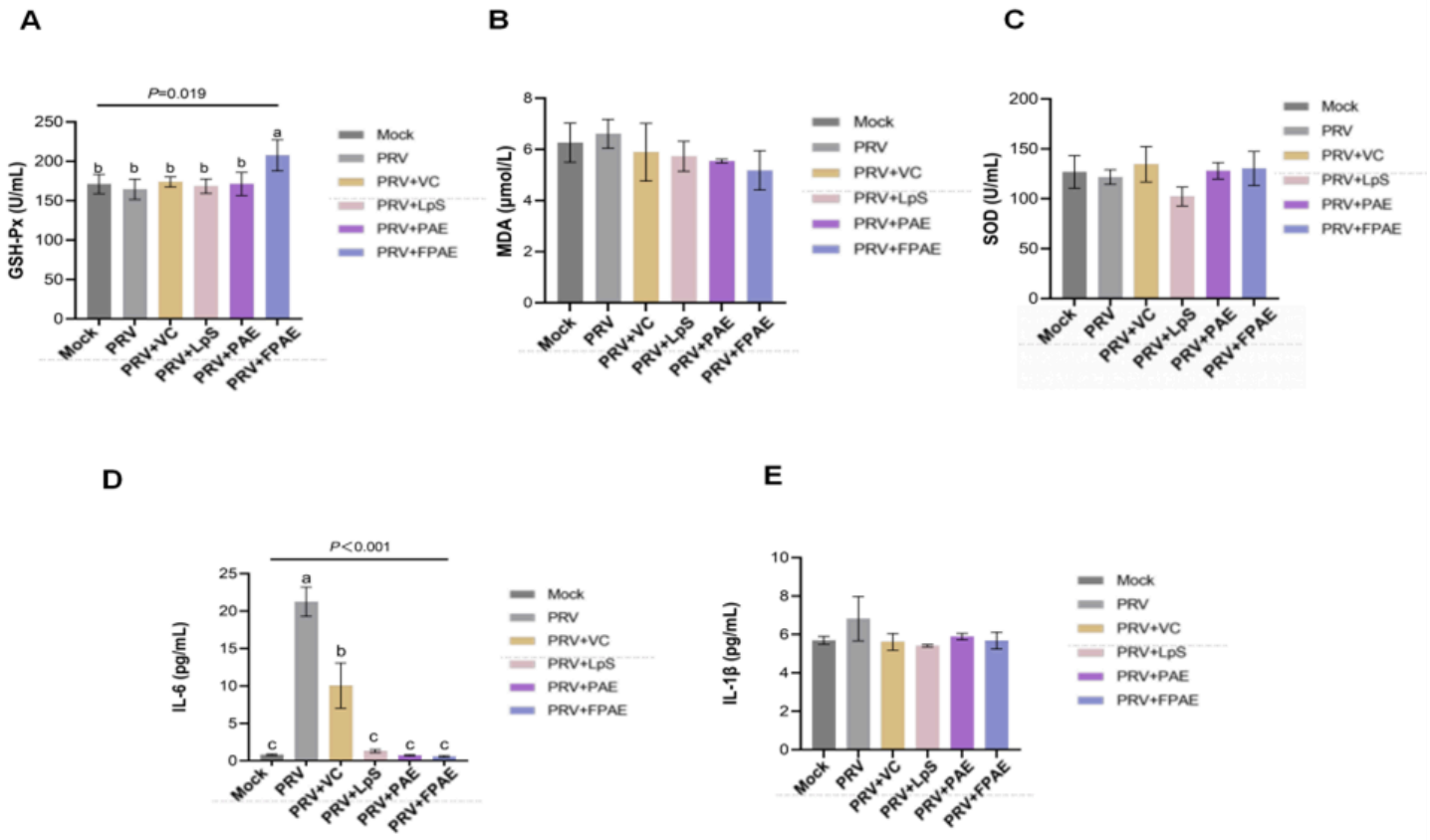

Figure 9

Effects of FPAE on serum antioxidant status and inflammatory cytokine levels in PRV-infected mice. **(A–C)** Serum antioxidant markers .**(A)** Glutathione peroxidase (GSH-Px) activity; **(B)** Malondialdehyde (MDA) content; **(C)** Superoxide dismutase (SOD) activity. **(D–E)**Serum inflammatory cytokine levels . **(D)** Interleukin-6 (IL-6); **(E)**Interleukin-1β (IL-1β). Data are presented as the mean ± SEM (n=3).Different lowercase letters (a, b, c...) indicate significant differences between groups ($P<0.05$), while identical letters or no letter indicate no significant difference ($P>0.05$).

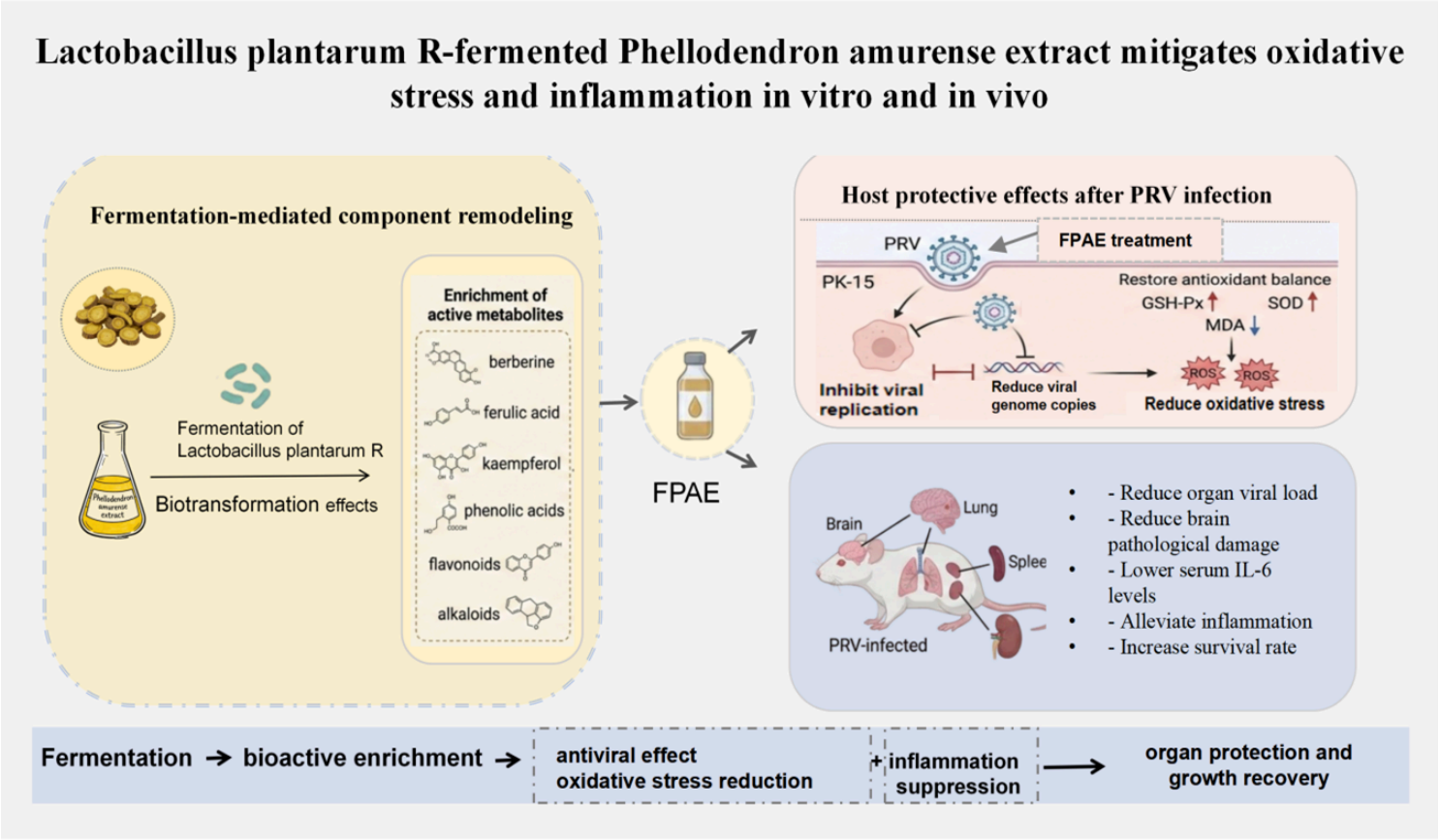

Figure 10

Schematic mechanism illustrating the protective effects of fermented Phellodendron amurense extract

Supplementary Files

This is a list of supplementary files associated with this preprint. Click to download.

- figureS1.tif
- tableS2.tif
- tableS3.tif
- tableS1.tif
- figureS2.tif